Asian Journal of Chemistry; Vol. 38, No. 1 (2026), 249-264
ASIAN JOURNAL OF CHEMISTRY
https://doi.org/10.14233/ajchem.2026.34783

Application of Chitosan-based Zirconia Hybrid Composite Functionalized with Multi-Walled Carbon Nanotubes for Efficient Removal of Humic Acid from Water Samples

J.T. PILUSA, C.P. MOKGOHLOA and L.E. MACEVELE*,

Department of Chemistry, University of Limpopo, Private Bag X1106, Sovenga 0727, South Africa

*Corresponding author: Tel: +27 15 268369; E-mail: lutendo.macevele@ul.ac.za

Received: 1 September 2025 *Accepted*: 20 December 2025 *Published online*: 31 December 2025 AJC-22245

Humic acid (HA) is abundant in soil and aquatic systems and can hinder wastewater treatment by affecting the removal of heavy metals and other contaminants. Herein, this study presents chitosan-zirconia (CTS-ZrO_2) composites doped with functionalized multi-walled carbon nanotubes (f-MWCNTs) for HA adsorption. The composites were characterized using TGA, BET, EDX, XRD, FTIR and SEM. Batch experiments assessed the effects of pH (2-8), adsorbent dosage (1-5 g L^{-1}), initial HA concentration (10-50 mg L^{-1}), contact time (5-240 min), temperature (25-40 ºC), ionic strength, reusability and binary systems. The CT-ZrO_2-f-MWCNTs composite exhibited a maximum adsorption capacity of 32.89 mg g^{-1} at pH 3, dosage of 2 g L^{-1}, initial HA concentration of 10 mg L^{-1} and 25 ºC, achieving 99.04% removal within 30 min. The adsorbent remained effective after five cycles and isotherm studies indicated that adsorption followed the Langmuir Type II model, suggesting multilayer adsorption.

Keywords: Chitosan, Zirconia, MWCNTs, Humic acid, Adsorption.

INTRODUCTION

Due to the rapid expansion of industries, an increasing number of water bodies are discovered to contain various types of emerging water contaminants [1]. A broad spectrum of these industries include hospitals, pharmaceuticals and municipalities of which due to a lack of efficient wastewater treatment plants, they dispose of their effluent in waterbodies [2]. Emerging contaminants (ECs) refers to substances that are not regulated in the environment and have detrimental effects on the environment and public health [2-4]. Examples of these contaminants include hormones, surfactants, heavy metals, gasoline, disinfectants, cosmetics, dyes, as well as phenols, like humic acid (HA) [5-8]. Humic acid, a model contaminant chosen for this study, is a large molecule made up of humic compounds, which are organic substances located in soil, natural bodies of water and sediments, consisting of phenolic, carboxyl and ketone groups [9,10]. The level of HA in water has a major impact on its quality as this has an influence on its colour, taste and odour [11]. Although the United States Environmental Protection Agency (USEPA) set a permitted limit of 0.1 mg L^{-1} in wastewater, the World Health Organization (WHO) approved a permitted phenolic content of 0.001 mg L^{-1} in drinkable water [12]. As a result, its removal is crucial to preserving public health and safety as well as wastewater infrastructure.

Recent reports have shown that adsorption is the most effective method for the removal of phenolic contaminants in wastewater, among other methods such as precipitation, ion exchange, filtration, reverse osmosis, coagulation and flocculation [4,10,13,14]. The adsorption approach is regarded as the most efficient method due to its broad applicability, environmental sustainability, high safety, rapid and straightforward process and economic benefits [15]. When compared to traditional methods, adsorption shows promising advantages due to its low-cost, high-efficiency solution for wastewater treatment; more especially when paired with an affordable and reusable adsorbent like chitosan [6].

Chitosan, a naturally occurring biopolymer, derived from the cell wall of crustaceans by deacetylation, attracted most researchers' attention, due to its physio-chemical properties which makes it a very effective adsorbent substance [16,17]. Its exceptional biocompatibility, adhesion ability and most importantly, its pronounced polycationic nature in acidic conditions are among the properties that stand out and prompted numerous researchers to utilise it for the elimination of emerging water contaminants [18]. However, with its remark-

able properties, chitosan suffers some drawbacks such as low porosity, low surface area and weak mechanical properties and this can be overcome by physical or chemical modifications [18]. The abundance of amino and hydroxyl groups in chitosan's structure allows its chemical and physical modification to improve physical solubility, surface area, crystallinity, morphology and electric charge [19,20]. Nonetheless, chitosan is easily protonated in some acidic solutions with pH less than 5.5, resulting in material loss and hard separation. The crosslinking procedure is one of the most common methods for improving the mechanical strength and chemical stability of chitosan in acidic conditions [15]. Glutaraldehyde is one of the mostly utilized chemical crosslinker, due to its ability to react at mild conditions, prevent swelling and enhancing chemical stability of the composite material. It reacts with the amino groups of chitosan to form Schiff bases, thereby covalently connecting chitosan chains to establish a stable network structure [21].

Zirconium(IV), a superior transition metal with a high positive charge characterized by its inert chemical and physical properties, photothermal stability, enhanced corrosion resistance, low toxicity and cost-effectiveness, also serves as a suitable agent for modification due to its capacity to create complex with chitosan [22,23]. Its excellent physical properties includes, increased strength, fracture resistance, a high melting point and decreased thermal conductivity [24]. Incorporation of zirconia (ZrO_2) into chitosan helps in the synthesis of a stable composite with improved structural features and high adsorption capacity [3]. It is a commonly utilized compound in wastewater management, characterized by its robust affinity, binding propensity and reduced leaching impact on water [23]. Elanchezhiyan *et al*. [22] synthesised glutaraldehyde cross-linked chitosan-ZrO_2 and demonstrated that incorporation of ZrO_2 significantly enhanced the physicochemical properties of chitosan as well as its adsorption capacity.

Carbon nanotubes, classified as single-walled and multi-walled, are a highly versatile carbon nanomaterial extensively utilized in wastewater treatment due to their exceptional thermal and chemical stability, substantial specific surface area and elevated porosity. However, they are hydrophobic, leading to their propensity to agglomerate in aqueous solutions, hence impeding their application in water [21]. To address this limitation, functional groups may be included into carbon nanotubes to improve hydrophilicity and enhance adsorption capacity. Multi-walled carbon nanotubes (MWCNTs) serve as superior adsorbent materials for diverse applications owing to their distinctive structural and chemical properties, including substantial pore volume, mechanical strength and potential for functionalization [25]. For instance, Khakpour & Tahermansouri [12] synthesized glutaldehyde crosslinked CTS-MWCNTs composite and applied adsorption in order to remove picric acid from water and recorded 157.85 mg g^{-1} adsorption capacity.

This work aims to investigate and employ chitosan as a biosorbent for the extraction of humic acid from aqueous solutions. Chitosan is first modified with glutaraldehyde as a cross-linker, ZrO_2, N-doped MWCNTs and/or f-MWCNTs and applied for the adsorption of humic acid under optimal conditions. These modifications create insoluble modified chitosan with improved contaminant removal capabilities [26]. In addition, the modification promotes regeneration while improving the stability, binding capacity and chemical stability of adsorbent [20,26]. An investigation of adsorption isotherms, kinetic models and thermodynamic parameters was performed using the experimental data and subsequently reported.

EXPERIMENTAL

All chemicals employed in this study were of analytical grade and were utilized without undergoing any additional purification processes. Distilled water was used for all the preparations of materials. Chitosan (CTS, degree of acetylation > 85), ZrO_2, MWCNTs, N-doped MWCNTs, humic acid (HA), NaCl, Na_2SO_4, KNO_3 and NaOH were purchased from Sigma-Aldrich. The reagent grade solvents namely acetic acid, ethanol, glutaraldehyde [$(CH_2)_3(CHO)_2$], sulphuric acid and nitric acid were purchased from Merck.

Functionalization of MWCNTs: MWCNTs (1 g) was mixed with 10 mL of HNO_3 and 30 mL of H_2SO_4 (1:3) in a 250 mL beaker, and the mixture was subsequently sonicated for 30 min. After that, the liquid was diluted with distilled water and filtered until pH 7. The functionalized MWCNTs were dried in an oven at 80 ºC.

Preparation of adsorbent composites: Synthesis of CTS, CTS-ZrO_2, CTS-ZrO_2-f-MWCNT/N-doped MWCNT were prepared by sol-gel synthesis. About 2 g of CTS flakes were dissolved in 120 mL of 5% CH_3COOH solution in a 250 mL beaker. Functionalized-MWCNTs/N-doped MWCNT and/or ZrO_2, 0.02 g and 5 g, respectively, were sonicated for 25 min after being introduced to 30 mL of 5% CH_3COOH. After combining the two solutions, f-MWCNTs/N-doped MWCNTs and/or ZrO_2 and CTS flakes were stirred for 24 h to ensure a homogenous mixture. Following a 24-h period of stirring, the solution was subsequently introduced dropwise into a beaker containing 500 mL of 0.50 M NaOH solution. This guaranteed the neutralization of the CH_3COOH present in the CTS gel, which caused the gel to congeal into homogeneous, spherical CTS composites gel beads. The beads were then filtered and washed with 200 mL of distilled water to remove the excess NaOH. Furthermore, the CTS composites beads were allowed to stand in 110 mL of 0.025 M glutaraldehyde solution at room temperature for a duration of 24 h and then filtered again and rewashed with 200 mL of distilled water. The CTS composites beads were dried at 40 ºC in an air-oven then ground to powder [3,27,28].

Characterization: Characterization techniques were employed to verify the successful synthesis of the nanocomposites. FTIR Spectrometer [Agilent Cary 600 series] acquiring FTIR spectra at a resolution of 10 cm^{-1} per 24 scans was utilized for confirming the incorporation of functional groups. TGA Q500 [V20.13 Build 39] was employed to analyse the thermal stability of the composites, at a ramping rate of 10 ºC min^{-1} under nitrogen atmosphere. The crystallinity of the composites was analysed using XRD diffraction [D8 XRD spectrometer] obtaining XRD peaks using Cu*K*α radiation (λ = 0.154 nm). Brunauer-Emmet-Teller instrument [Micromeritics ASAP 2020] was used to determine the surface area and porosity of the

composites. The surface morphology of the composites was examined using SEM [Sigma 500 VP, Zeiss SEM with Gemini FE-SEM column] at different magnifications ranging from 10,000× to 50,000× and elemental composition was determined using EDX spectroscopy [EDΛX, Z1 Analyzer]. The images were captured using the SmartSEM® (Carl Zeiss, Germany) software.

Point of zero charge: The point of zero charge (PZC) was determined as proposed by the method carried by Borba *et al*. [29]. The method employed was pH-drift method which was done by dispersing 50 mg of composites into 20 mL of 0.05 M NaCl at different pH ranges of 2.0–9.0 varied using 0.1 M HCl and NaOH. The mixture was stirred at 120 rpm by magnetic stirrer [EINS'sCI, E-MS3-H2-D] for 24 h at room temperature while enclosed by aluminium foil. The final pH was measured by a pH meter [PC 7, XS] and recorded. The PZC was derived by plotting the difference in pH (final pH – initial pH) against initial pH.

Batch adsorption studies: Factors affecting adsorption *viz*. solution pH, dosage, adsorbate's initial concentration, temperature, contact time, ionic strength and binary system for the removal of HA from aqueous solutions were studied. A stock solution of 1000 mg L^{-1} HA spiked water sample were prepared and further diluted to 10-50 mg L^{-1} to prepare standard solutions and generated standard curve. The effect of pH on the adsorption of HA was conducted by adjusting the pH of the solution from a range of 2 to 8 using 0.1 M HCl and 0.1 M NaOH. The effect of dosage was investigated by adjusting the amounts of the adsorbent within the range of 20 to 100 mg in a 20 mL solution (1, 2, 3, 4 and 5 g L^{-1}) of HA at pH 3. To investigate the effect of concentration, the initial concentrations of HA were systematically varied within the range of 10 to 50 mg L^{-1}, kept at pH 3 and dosage of 2 g L^{-1}. The study of the effect of contact time was performed by varying exposure time of the composites to HA solution from 5 to 240 min in which 2 g L^{-1} dosage solutions of 10 mg L^{-1} concentrations kept at pH 3. The effect of temperature was investigated by adjusting the temperature of the HA solution within the range of 25 to 40 ºC and kept at optimum conditions. The study of each adsorption parameters was achieved by optimising other adsorption parameters for the maximum removal efficiency during batch adsorption. The study of the effect of ionic strength was evaluated by preparing 10 mg L^{-1} HA solution containing 10, 20 and 30 mg L^{-1} of Cl^-, SO_4^{2-} and NO_3^- ions, respectively, prepared from NaCl, Na_2SO_4 and KNO_3 and compared removal efficiency with the one without ionic species. Consequently, the study of binary system was conducted by immersing 10 mg L^{-1} casein from bovine milk in 10 mg L^{-1} HA and applied adsorption at optimum conditions. Ultraviolet/Visible spectroscopy [Agilent Technologies Cary 60 UV-vis] was used to determine the quantities of adsorbed HAs in the filtrate after filtering with 0.45 μm nylon membrane by measuring the absorbance at a wavelength of 283 nm. Finally, the final concentrations of HA were used to obtain removal efficiency (%) and adsorption capacity q_e (mg g^{-1}) as follows:

$$\text{Removal (\%)} = \frac{C_o - C_e}{C_o} \times 100 \quad (1)$$

$$q_e = \frac{(C_o - C_e) \times V}{m}$$

where C_o and C_e (mg L^{-1}) represent the initial and final concentrations of HA, respectively; V (L) indicates the volume of HA solution; m (g) denotes the weight of adsorbent

Desorption and reuse of CTS and CTS composites: Desorption of adsorbed HA was carried out by immersing the adsorbent-adsorbate (CTS composite-HA) complex in 50 mL NaOH solution and continuously stirred at 120 rpm for 2 h at room temperature. After filtering off the desorbed HA, the CTS composites was washed with distilled water and allowed to dry at 40 ºC. Chitosan and CTS composites were then reused again for adsorption of HA under optimal conditions as discussed above for 5 cycles measuring the adsorbed amount of HA in each cycle. Ultraviolet/Visible spectroscopy [Agilent Technologies Cary 60 UV-vis] was used to determine the quantities of adsorbed HAs by comparing the initial and final concentrations when equilibrium was reached. Finally, the final concentrations of HA were used to obtain removal efficiency (%) and adsorption capacity q_e (mg g^{-1}) as mentioned above.

Statistical data analysis: Each set of experiment was conducted in replicates to ensure the reliability and reproducibility of the results. This is to mitigate the influence of outliers and experimental variability. The data are presented as the average and standard deviation (mean ± SD) of three independent experiments, unless specified differently. The model equation's coordination constants and removal efficiencies were computed with Excel text tools. Data analysis and graphical depiction were conducted utilising OriginPro 2025 software.

RESULTS AND DISCUSSION

Fourier transform infrared spectroscopy: The FTIR spectra of CTS, CTS-ZrO_2, CTS-ZrO_2-N-doped MWCNTs and CTS-ZrO_2-f-MWCNTs composites are shown in Fig. 1. FTIR was employed to determine the successful synthesis of the composites outlining the presence of characteristic functional groups and hence giving the chemical structures of the composites. Analysis of CTS shows a C-O bending vibration that can be attributed to the peak at 1100-1000 cm^{-1}. The characteristic peaks at 1440, 1651 and 1712 cm^{-1} are determined to be the C-N stretching vibration, the N-H amino bending vibration and the C-O carboxyl group stretching vibration, respectively [12]. In addition, the broad peak at 3524-2700 cm^{-1} along with the peak at 2900 cm^{-1} is indicative of the O-H stretching vibration and the aliphatic C-H stretching vibration of methyl (-CH_3) group, respectively [30]. The vibrations described above are detected in CTS and all composites (CTS-ZrO_2, CTS-ZrO_2-N doped MWCNTs, CTS-ZrO_2-f-MWCNTs), demonstrating that CTS is present in all composites without undergoing any phase changes. The incorporation of ZrO_2 into CTS is accompanied by the appearance of the intense absorption bands observed at 523 cm^{-1} and 767 cm^{-1} that can be attributed to the Zr-O-Zr and Zr-O stretching vibrations, respectively. The reaction between the oxygen of ZrO_2 and the amino group of CTS, is responsible for the

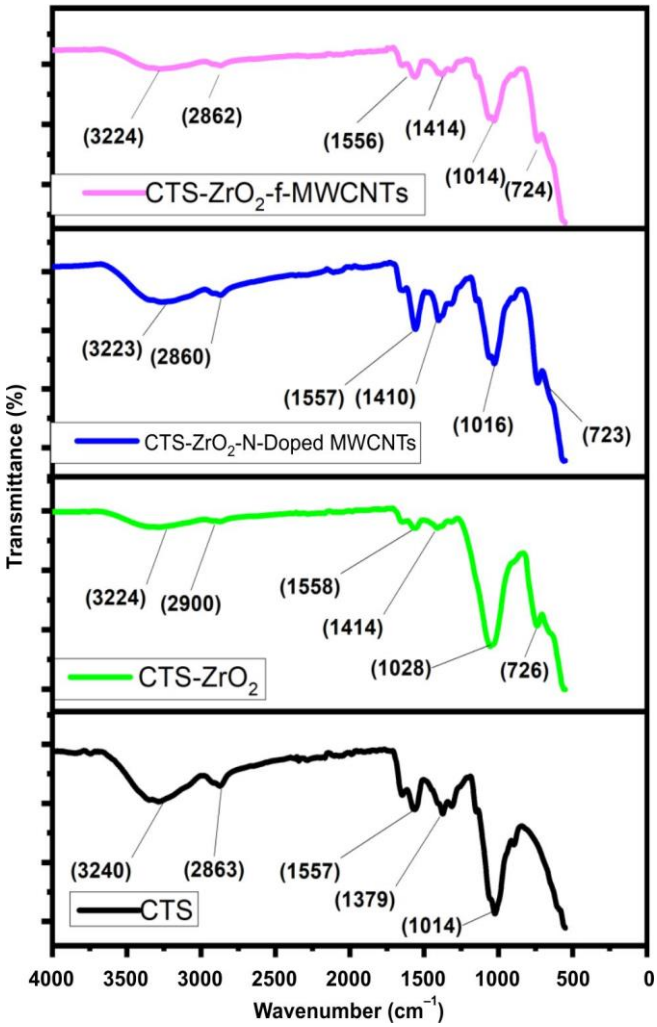

Fig. 1. FTIR spectra of CTS and CTS composites

notable intensity of subsequent vibration peaks as recorded in literature [22,24]. This observation justify the presence of ZrO_2 within the CTS-ZrO_2, CTS-ZrO_2-N doped MWCNTs, CTS-ZrO_2-f-MWCNTs composites suggesting the successful modification and synthesis of CTS/MWCNTs/ZrO_2 composite.

Scanning electron microscopy (SEM): The SEM images of CTS, CTS-ZrO_2, CTS-ZrO_2-N-doped MWCNTs and CTS-ZrO_2-f-MWCNTs composites are shown in Fig. 2. As it can be seen from Fig. 2a, CTS is observed to have a smooth surface with less porosity. However, the introduction of ZrO_2, in comparison to MWCNTs, make the surface of CTS rough and more porous, as depicted in Fig. 2b. This is due to its strong interaction with CTS. The combination of all three, CTS, ZrO_2 and N-doped/f-MWCNTs, preserved all which have been mentioned. The addition of each component to CTS increased overall available sites for adsorption, as it can be seen in Fig. 2c-d, thus enhancing adsorption. Furthermore, the addition of ZrO_2 to the CTS matrix resulted in an uneven, granular and above all highly porous composite surface [22, 24]. The MWCNTs in these images are seen to be rope-like and cylindrical in shape. The SEM pictures indicate the locations of the MWCNTs insertion and dispersion within the CTS matrix, thus confirming the successful synthesis of the composites.

Energy dispersive X-ray (EDX): Fig. 3 shows the energy dispersive X-ray (EDX) spectroscopy of CTS, CTS-ZrO_2, CTS-ZrO_2-N-doped MWCNTs and CTS-ZrO_2-f-MWCNTs composites. As shown in Fig. 3, EDX spectra of the composites reveals the presence of carbon, oxygen and nitrogen in CTS and all CTS composite, confirming the presence of the CTS functional groups. Incorporation of ZrO_2 is confirmed by the presence of a more intense peak with a high Zr content as observed from Fig. 3b-d, confirming the successful encapsulation of zirconium ions into the chitosan composite as noted in literature [22]. The introduction of N-doped MWCNTs and functionalized MWCNTs into CTS did not introduce different atoms compared to those already present, but increased the atomic percentage as it can be seen in Fig. 3c-d. Higher oxygen and carbon content is observed in CTS (Fig. 3a) than in other CTS composites.

X-ray diffraction (XRD): Fig. 4 shows diffraction patterns of CTS, CTS-ZrO_2, CTS-ZrO_2-N-doped MWCNTs and CTS-ZrO_2-f-MWCNTs composites. Chitosan shows characteristic peak at around $2\theta = 20.03^{\circ}$, corresponding to (110) reflection plane. Incorporation of ZrO_2 into CTS, this reflection plane (110) shifted to an upper region at $2\theta = 28.4^{\circ}$, which can be accounted for the interaction of CTS with monoclinic ZrO_2 altering CTS crystalline structure and can be observed in all composites (CTS-ZrO_2, CTS-ZrO_2-N-doped MWCNTs and CTS-ZrO_2-f-MWCNTs) comparable to the work reported in literature [12,21,22]. These composites show additional characteristic peaks at 2θ values of around 31.7° and 50.33° corresponding to (111) and (221) reflection planes, respectively, of monoclinic ZrO_2 [3]. Incorporation of MWCNTs, however, did not show significant impact as shown by the diffraction pattern of CTS-ZrO_2-N-doped MWCNTs and CTS-ZrO_2-f-MWCNTs and this is due to their characteristic peak overlapping with that of CTS. The study thus reveals successful modification of CTS crystalline structure with the uniform dispersion of ZrO_2 throughout the CTS matrix as confirmed with less intense peaks corresponding to ZrO_2 than of CTS.

Thermal studies: The TGA thermograms of CTS, CTS-ZrO_2, CTS-ZrO_2-N-doped MWCNTs and CTS-ZrO_2-f-MWCNTs composites are shown in Fig. 5. The curve of CTS, CTS-ZrO_2, CTS-ZrO_2-N-doped MWCNTs and CTS-ZrO_2-f-MWCNTs exhibit weight loss of about 16%, 4%, 8% and 6%, respectively, at 40-180 ºC which can be attributed to the evaporation of moisture from the composites [22,31]. Subsequently, a gradual trend is observed within the temperature range of 180 to 420 ºC, during which the weight loss percentages are approximately 54%, 24%, 18% and 18% for CTS, CTS-ZrO_2, CTS-ZrO_2-N-doped MWCNTs and CTS-ZrO_2-f-MWCNTs, respectively. This weight loss can be attributed to the degradation of CTS groups. At temperatures reaching 900 ºC, a weight loss of approximately 20%, 1%, 13% and 12% for CTS, CTS-ZrO_2, CTS-ZrO_2-N-doped MWCNTs and CTS-ZrO_2-f-MWCNTs, respectively, was observed, attributed to the degradation of crosslinked CTS and MWCNTs groups [22]. The estimated total mass loss at 900 ºC is approximately 90% for CTS, 29% for CTS-ZrO_2, 39% for CTS-ZrO_2-N-doped MWCNTs and 36% for CTS-ZrO_2-f-MWCNTs. Consequently, thermal analysis demonstrates the advantage of CTS-ZrO_2 composites compared to their parent compound CTS.

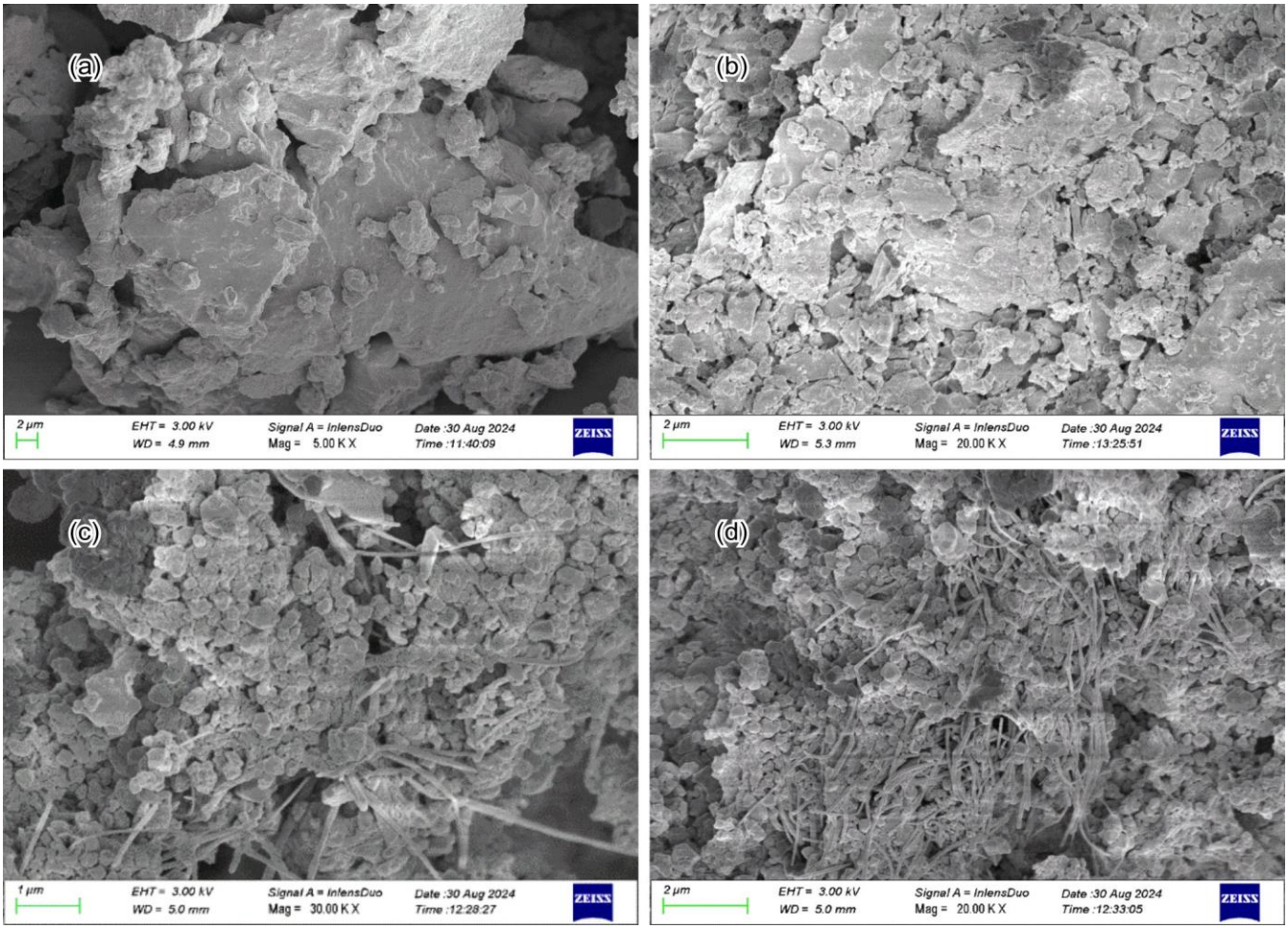

Fig. 2. SEM images of (a) CTS, (b) CTS-ZrO_2, (c) CTS-ZrO_2-f-MWCNTs and (d) CTS-ZrO_2-N-doped MWCNTs

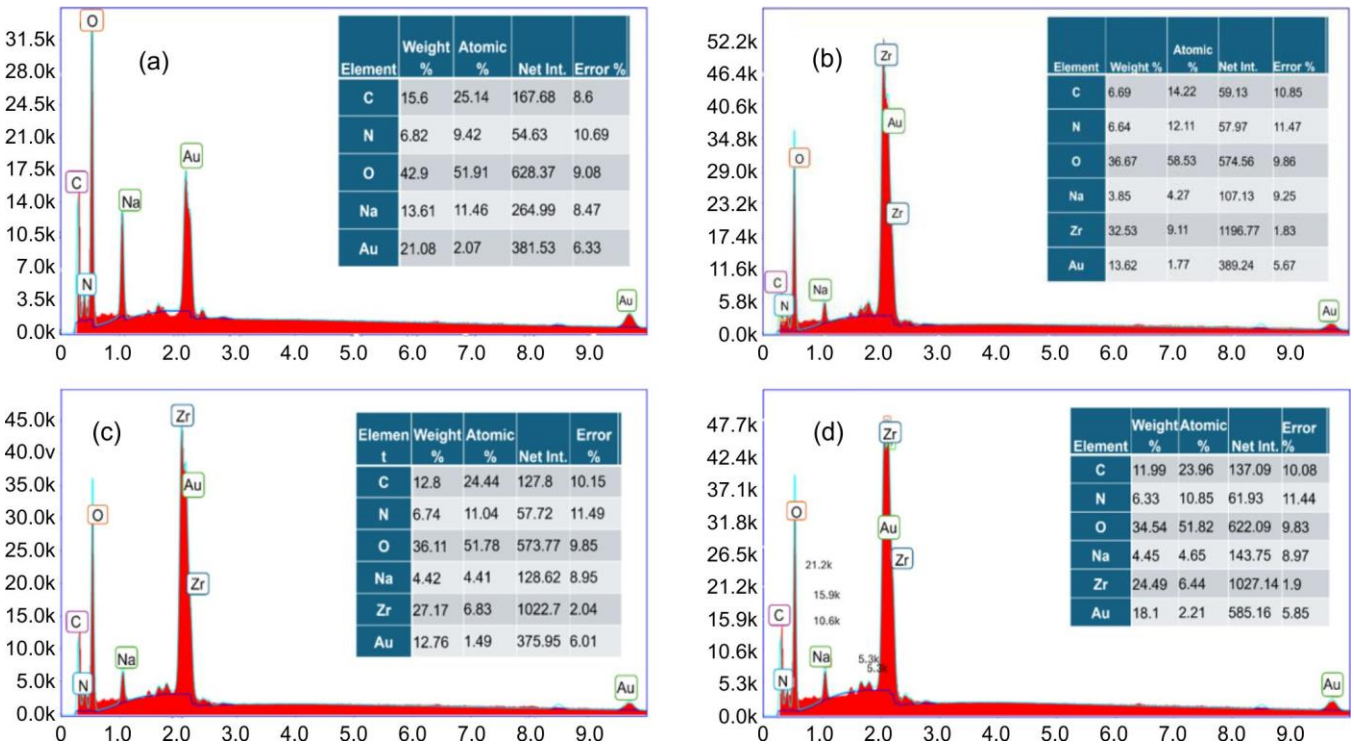

Fig. 3. EDX spectra of (a) CTS, (b) CTS-ZrO_2, (c) CTS-ZrO_2-f-MWCNTs and (d) CTS-ZrO_2-N-doped MWCNTs

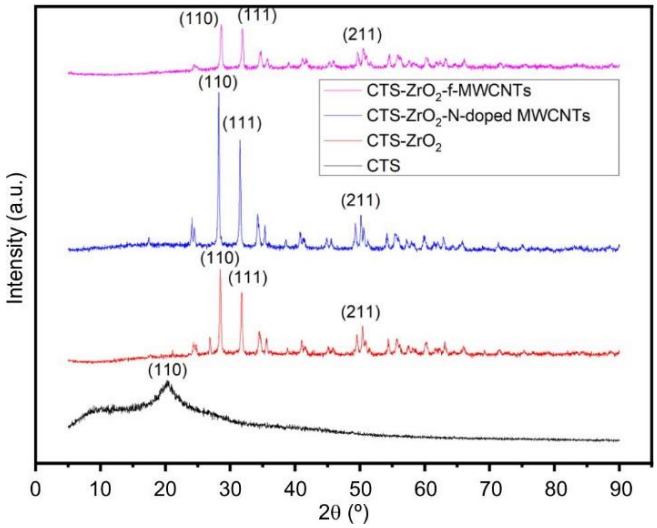

Fig. 4. XRD pattern of CTS and CTS composites

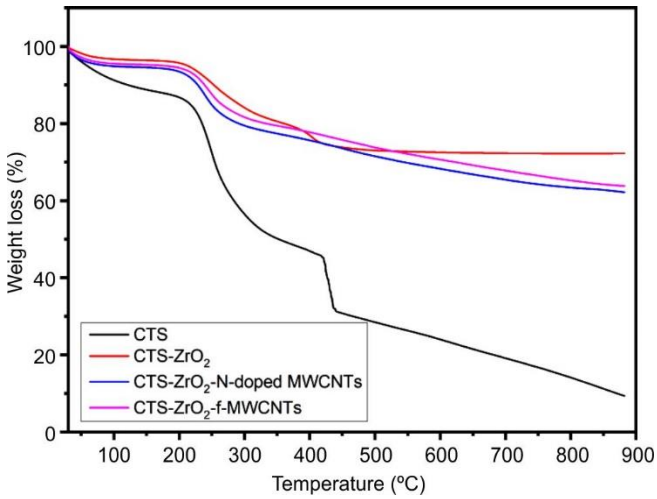

Fig. 5. TGA curves of CTS, CTS-ZrO_2, CTS-ZrO_2-N-doped MWCNTs and CTS-ZrO_2-f-MWCNTs

Brunauer-Emmett-Teller (BET): Fig. 6 shows the nitrogen adsorption-desorption isotherms and Barrett-Joyner-Halenda (BJH) pore size distributions of CTS, CTS-ZrO_2, CTS-ZrO_2-N-doped MWCNTs and CTS-ZrO_2-f-MWCNTs composites. The surface area and pore size assessment of the synthesized composites were conducted utilising the BET method. All of the materials displayed nitrogen adsorption–desorption isotherms that exhibited Type IV features with an

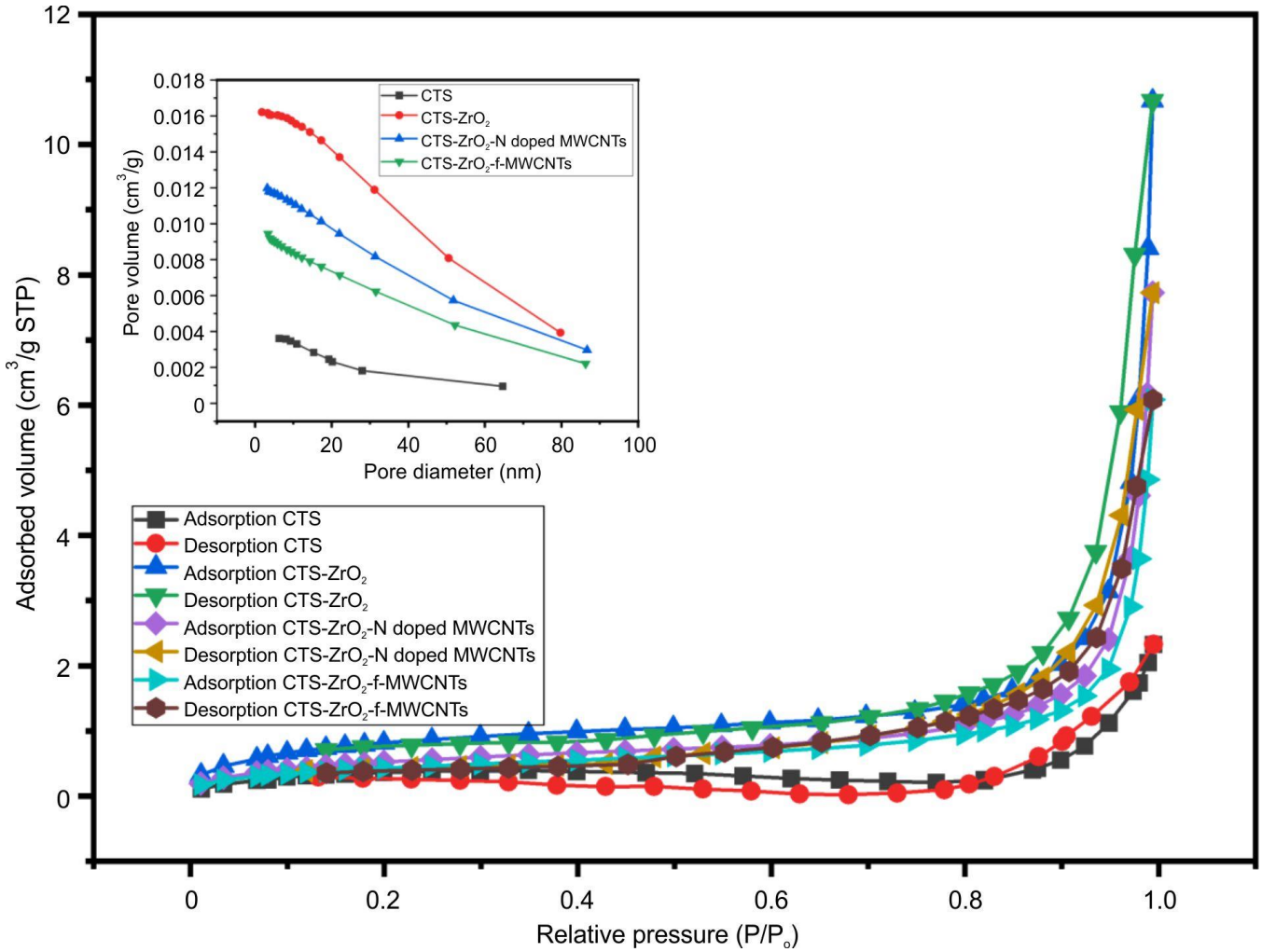

Fig. 6. The BET curves of nitrogen gas adsorption and desorption isotherms and BJH pore size distribution (inset) of CTS, CTS-ZrO_2, CTS-ZrO_2-N doped MWCNTs and CTS-ZrO_2-f-MWCNTs

3 hysteresis loop, indicating mesoporous structures, as per the usual IUPAC categorization [21,32]. The more inclined/steep region at P/P_0 of around 0.9-1.0, is the characteristic feature of Type-IV isotherm [33]. Table-1 shows the BET surface area and pore volume of CTS, CTS-ZrO_2, CTS-ZrO_2-N-doped MWCNTs and CTS-ZrO_2-f-MWCNTs composites. The BET surface area of CTS, CTS-ZrO_2, CTS-ZrO_2-N doped MWCNTs and CTS-ZrO_2-f-MWCNTs were 1.2823, 2.9530, 1.9572 and 1.6041, respectively. That is, incorporation of ZrO_2 into CTS, increased the available surface area of the composites. However, the incorporation of MWCNTs (functionalized and N-doped) into CTS-ZrO_2 adsorbent composite seem to have reduced the overall surface area as more active sites are occupied on the CTS composite, although CTS-ZrO_2-N doped MWCNTs composite had a higher surface area. Interestingly, CTS-ZrO_2-f-MWCNTs composite performed better in adsorption studies which could be due to the improved surface area and properties of the functional materials. Furthermore, the average pore volume of CTS, CTS-ZrO_2, CTS-ZrO_2-N doped MWCNTs and CTS-ZrO_2-f-MWCNTs showed the same trend, with the incorporation of ZrO_2 into CTS increasing the pore volume making the CTS composites efficient for trapping the adsorbates and thus high removal efficiency.

TABLE-1
THE BET SURFACE AREA, AVERAGE PORE SIZE AND PORE VOLUME OF CTS, CTS-ZRO$_2$, CTS-ZRO$_2$-N DOPED MWCNTS AND CTS-ZRO$_2$-F-MWCNTS

Adsorbent composite	BET surface area (m^2/g)	Pore volume (cm^3/g)
CTS	1.2823	0.001781
CTS-ZrO_2	2.9530	0.004981
CTS-ZrO_2-N doped MWCNTs	1.9572	0.003800
CTS-ZrO_2-f-MWCNTs	1.6041	0.003084

Point of zero charge of composite adsorbents: Fig. 7 shows the pHpzc of CTS, CTS-ZrO_2, CTS-ZrO_2-N-doped MWCNTs and CTS-ZrO_2-f-MWCNTs composites. All composite materials, exhibited a similar pHpzc of approximately 7.8, indicating that surface charge behaviour is largely governed by the chitosan matrix [34]. At pH values lower than the pHpzc, the surface becomes positively charged due to protonation of surface functional groups, favouring electrostatic attraction of anionic species. Conversely, at pH values above the pHpzc, the surface carries a net negative charge due to deprotonation, enhancing adsorption of cationic species [35]. The incorporation of ZrO_2 and functionalized or N-doped MWCNTs did not significantly shift the pHpzc, but slight differences in ΔpH trends at acidic pH suggest modifications to surface buffering capacity and proton affinity, which could influence adsorption kinetics and capacity through mechanisms beyond simple electrostatic interactions [29].

Adsorption experiments: The effect of pH (ranging from 2 to 8) on the removal of HA from aqueous solutions under optimal conditions is illustrated in Fig. 8. The experimental results of adsorption of HA suggests that as pH increases from 2 to 3, amount of adsorbed HA increases, which can be related to the less solubility of HA in the acidic media [28,36]. At a pH of 3, the adsorption of HA onto CTS, CTS-ZrO_2, CTS-

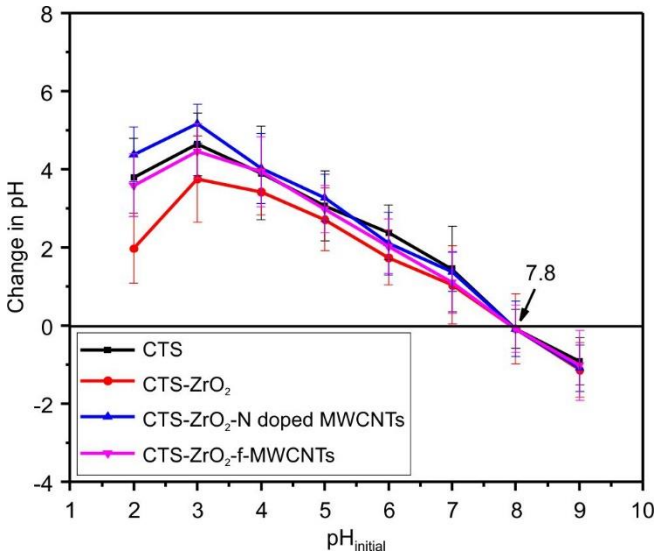

Fig. 7. Point of zero charge of CTS, CTS-ZrO_2, CTS-ZrO_2-N doped MWCNTs, CTS-ZrO_2-f-MWCNTs

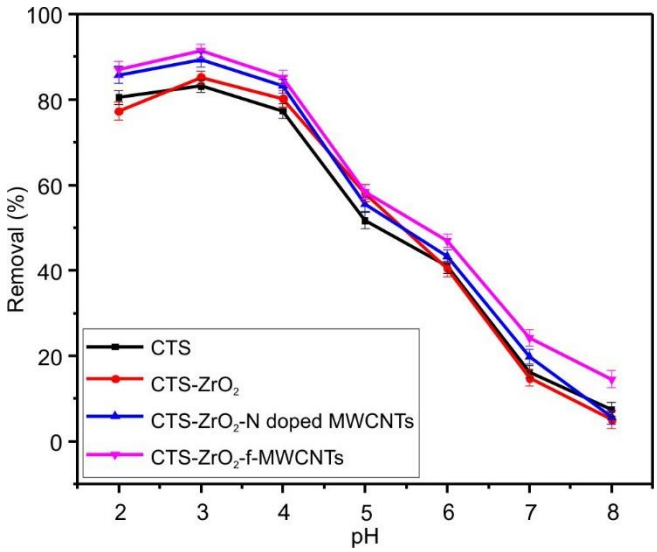

Fig. 8. Effect of pH on the adsorption of HA from aqueous solution (experimental conditions: dosage, 0.333 g L^{-1}; HA concentration, 50 mg L^{-1}; contact time, 30 min; at room temperature)

ZrO_2-N-doped MWCNTs and CTS-ZrO_2-f-MWCNTs demonstrates the highest removal efficiencies of 83.14%, 89.36%, 85.2% and 94.04%, respectively. This phenomenon can be attributed to the protonation of COOH groups, which results in reduced solubility for both the adsorbate (HA) and the adsorbent. Humic acid is characterized by functional group COOH and has a pK_a value of 3.1, which depends on its source. Therefore, the pK_a value of HA suggests that at solution pH < 3.1 the carboxyl group remains protonated and above that it become deprotonated and as such its solubility is influenced [36]. However, as pH increases from 4 to 8, the amount of HA adsorbed on CTS adsorbent decreases. This phenomenon can be attributed to the fact that at pH levels exceeding 3.1, HA undergoes deprotonation, resulting in the formation of humate anions. These anions exhibit increased solubility in aqueous solutions. Consequently, the stronger bond between the adsorbate and water must dissociate prior to the

occurrence of adsorption [12]. Increasing electrostatic repulsions between HA and the adsorbents' surface negative charge (at pH > pHpzc) could also be the cause of this [11].

Dosage studies were conducted to assess the adsorption percentage of HA from 50 ppm HA aqueous solution on CTS and CTS composites as shown by Fig. 9. This was achieved by varying dosage from 1-5 g L^{-1}. The study illustrates that as the dosage increases from 1-2 g L^{-1}, HA adsorption capacity increase, which can be attributed to more available adsorption sites for unretained HA [10]. However, as amounts of adsorbent is further increased, HA adsorption capacity starts to decrease because the adsorption sites become unsaturated during the adsorption process, due to availability of more adsorption sites [30]. The adsorbate (HA) migrates about the adsorption sites without reaching equilibrium and/or there is a competition among the adsorption sites [10]. At a dosage of 2 g L^{-1} for CTS, CTS-ZrO_2, CTS-ZrO_2-N-doped MWCNTs and CTS-ZrO_2-f-MWCNTs, the maximum removal efficiencies for HA are observed to be 66.64%, 96.69%, 96.7% and 97.87%, respectively. This phenomenon can be explained by the attainment of a saturation point, at which all available adsorption sites are fully occupied, thereby preventing any further adsorption of additional adsorbates [37].

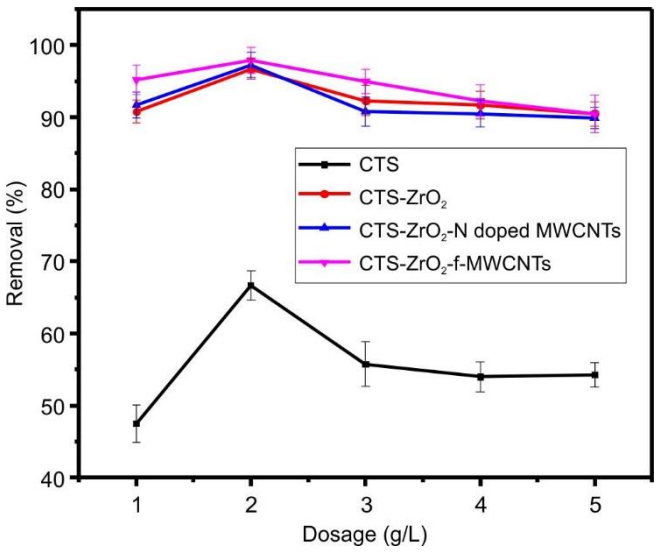

Fig. 9. Effect of adsorbent dosage on the adsorption of humic acid from aqueous solution (experimental conditions: pH = 3; humic acid concentration, 50 mg L^{-1}; contact time, 30 min at room temperature)

Fig. 10 shows the effect of initial concentration of HA on its removal from aqueous solution at optimal conditions. The effect of the initial concentration of HA was investigated by varying its concentration between 10 and 50 mg L^{-1}, while maintaining a constant dosage. The experimental results indicate that an increase in the concentration of HA in the aqueous solution corresponds with a decrease in the effectiveness of HA removal. This phenomenon can be attributed to the observation that as the concentration of HA increases while the dosage remains constant, a reduced number of adsorption sites become available. This occurs because the HA molecules occupy these sites, resulting in a lowered adsorption capacity. At a low concentration of 10 ppm of HA, the removal efficiencies observed for CTS, CTS-ZrO_2, CTS-ZrO_2-N-doped MWCNTs and CTS-ZrO_2-f-MWCNTs are 93.45%, 97.87%, 98.16% and 99.04%, respectively.

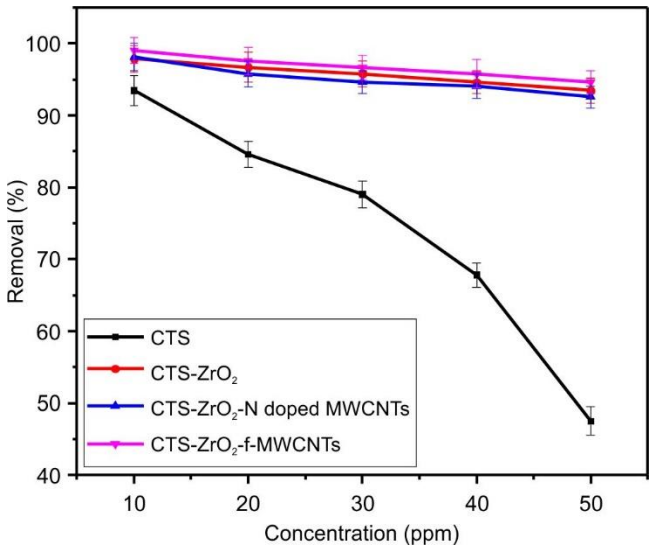

Fig. 10. Effect of initial concentration of HA on adsorption of HA from HA aqueous solution (experimental conditions; pH = 3; dosage 2 g L^{-1}; contact time, 30 min, at room temperature)

The isotherm of any adsorption system is a mathematical equation that relates the quantity of the adsorbent at a constant temperature to the amount of adsorbate on its surface [6]. It's an indication of how an adsorbate transfers to the adsorbent from an aqueous solution when an equilibrium is reached. This study clarifies the mechanism of adsorption through the application of the Langmuir and Freundlich isotherm models, along with the corresponding constant values that characterise the surface properties and affinity of the adsorbent.

The Langmuir isotherm (s) and its linearized form are expressed based on the following equations:

$$q_e = \frac{bq_m C_e}{1 + bC_e} \quad (2)$$

$$\frac{C_e}{q_e} = \frac{1}{bq_m} + \frac{C_e}{q_m} \quad \text{Type 1}$$

$$\frac{1}{q_e} = \frac{1}{q_m} + \frac{1}{bq_m C_e} \quad \text{Type 2}$$

$$q_e = q_m - \frac{q_e}{bC_e} \quad \text{Type 3}$$

$$\frac{q_e}{C_e} = bq_m - bq_e \quad \text{Type 4}$$

where b (L mg^{-1}) depicts the Langmuir equilibrium constant, q_e (mg g^{-1}) represent the equilibrium adsorption quantity, C_e (mg L^{-1}) is the equilibrium concentration of adsorbate in the solution, q_m (mg g^{-1}) refers to the maximum adsorption capacity or the theoretical monolayer saturation capacity.

The Freundlich isotherm characterises the heterogeneity of surfaces and describes the relationship between the concentration of adsorbate and the energy of the active sites through an exponential function [38]. It is valid for both multi-layer and heterogeneous molecule adsorption. The linearized representation of the Freundlich equation is as follows:

$$\ln q_e = \ln K_f + \frac{1}{n}\ln C_e \quad (3)$$

where K_f (L mg^{-1})(L g^{-1})^n refers to an empirical constant associated with the adsorption capacity of the adsorbent, which varies in accordance with the surface heterogeneity and the affinity of the material and n represents the strength of the adsorption. The plot of ln q_e against C_e gives a linear relationship where constant n is estimated from slope and K_f from the intercept.

Figs. 11-14 show the Langmuir Type 1, 2, 3 and 4 plot of CTS and CTS-ZrO_2-f-MWCNTs, respectively. Table-2 contains the calculated values of the Langmuir and Freundlich isotherm parameters. From the Langmuir models, the Type 2 equation's regression coefficients (R^2) average are higher than those of the other three forms, indicating that it is the best form for interpreting experimental data of all composites. It indicates that the adsorbent's surface active sites are uniform and that the monolayer's adsorption process necessitates an equivalent activation energy for every species [6]. In addition, the agreement of the experimental data and those predicted by Langmuir Type 2 model indicates that the adsorption is governed by physical adsorption. Table-3 shows the comparison of CTS-ZrO_2-f-MWCNTs composite adsorbent with other adsorbents on the removal of HA at various conditions. As shown in Table-3, the maximum adsorption by Langmuir Type 2 was 32.89 mg g^{-1} by the CTS-ZrO_2-f-MWCNTs composite was the highest compared other adsorbents reported in literature during the removal of HA in aqueous solution. The CTS-ZrO_2-f-MWCNTs composite was also able to remove 99.04% of humic acid at a less time compared with other reported adsorbents at room temperature.

The Freundlich models exhibit lower correlation coefficients in comparison to the Langmuir models for CTS and CTS-ZrO_2-f-MWCNTs, which recorded values of 0.9351 and 0.9893, respectively (Fig. 15). This indicates that the Freundlich models are not appropriate for interpreting the experimental data, as anticipated, given that the adsorbents employed have been shown to possess homogeneous surfaces

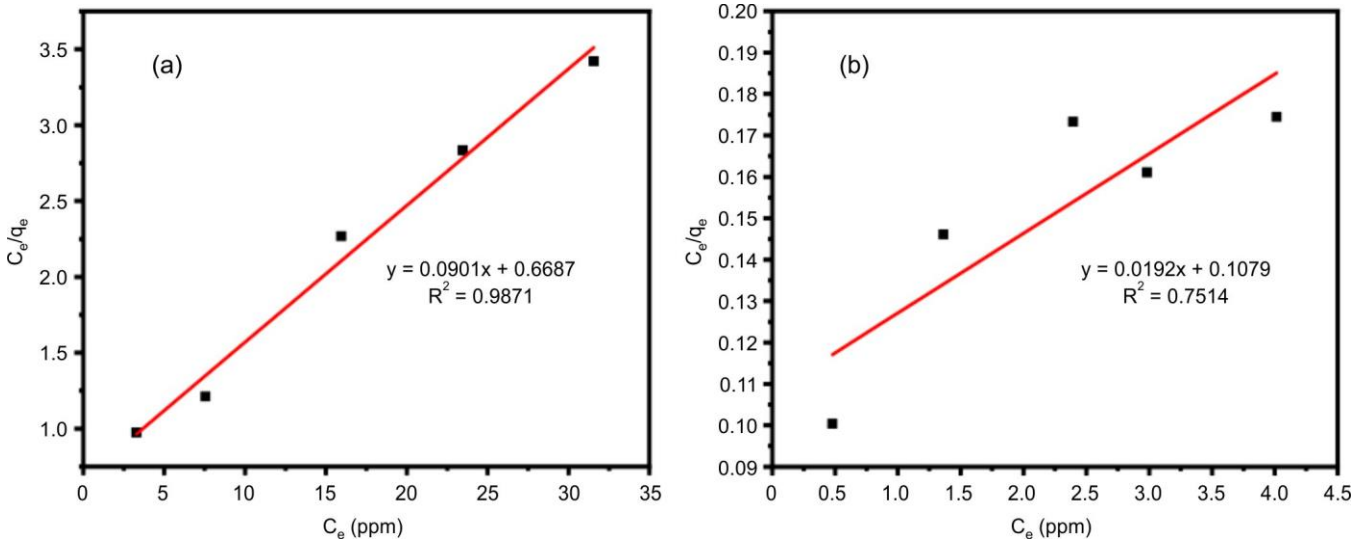

Fig. 11. Langmuir Type 1 plot of CTS (a) and CTS-ZrO_2-f-MWCNTs (b)

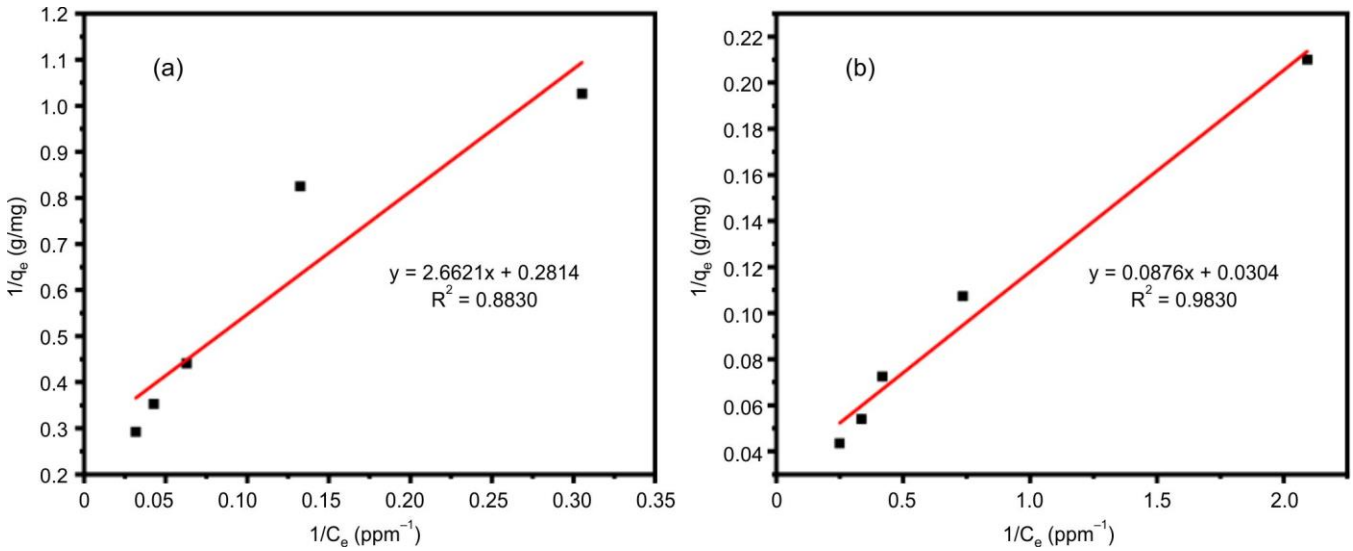

Fig. 12. Langmuir type 2 plot of CTS (a) and CTS-ZrO_2-f-MWCNTs (b)

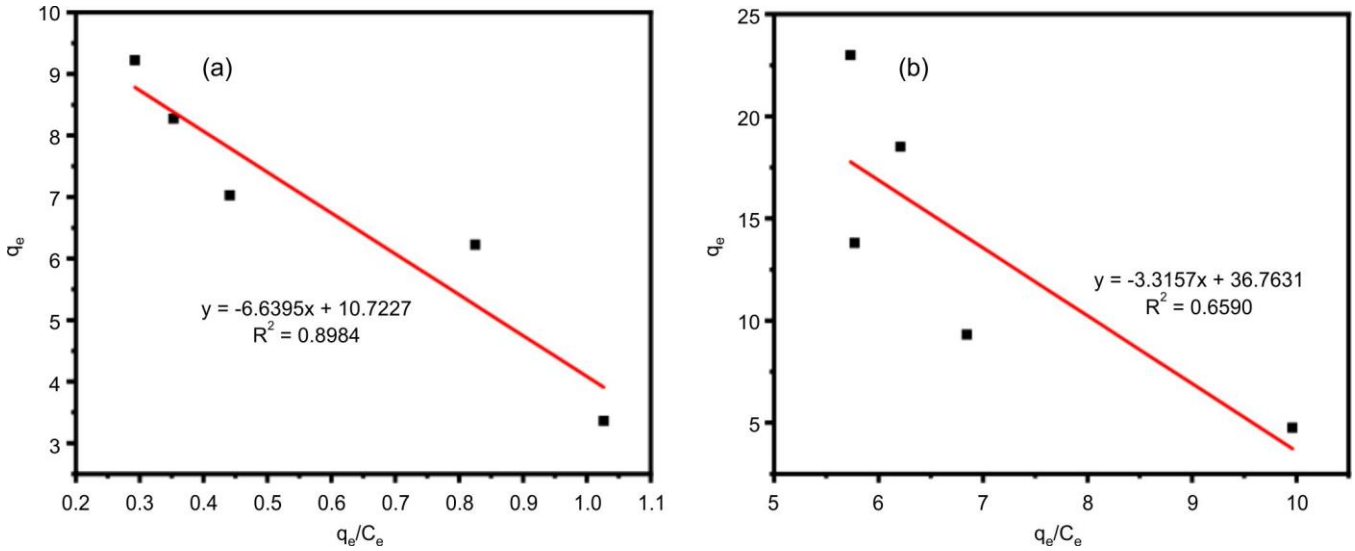

Fig. 13. Langmuir Type 3 plot of CTS (a) and CTS-ZrO_2-f-MWCNTs (b)

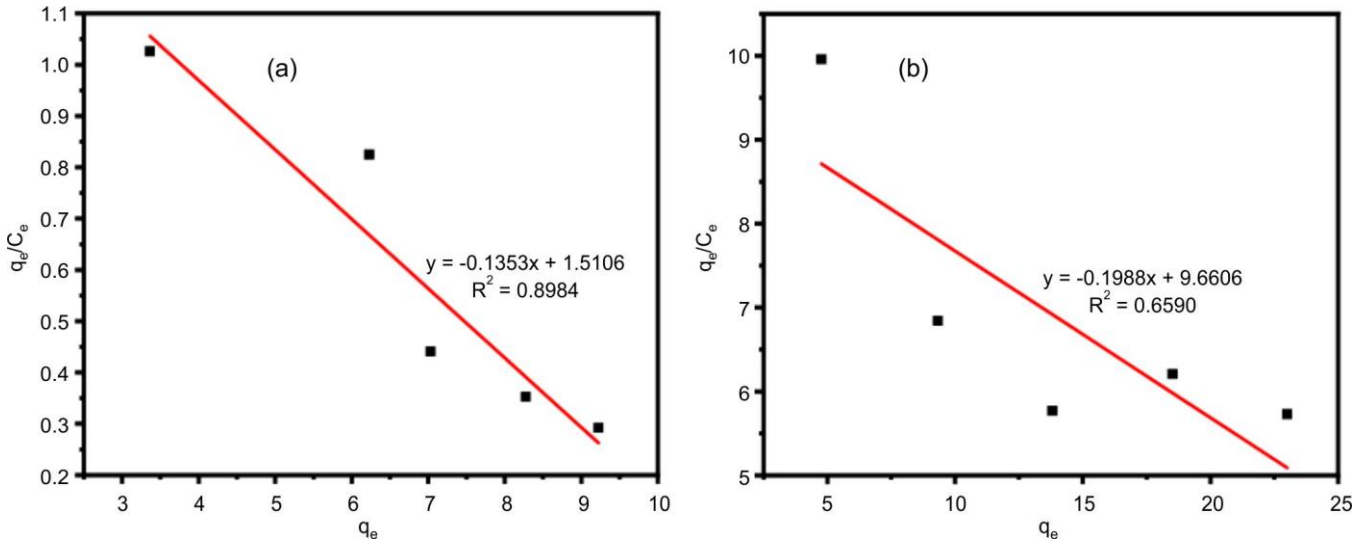

Fig. 14. Langmuir Type 4 plot of CTS (a) and CTS-ZrO_2-f-MWCNTs (b)

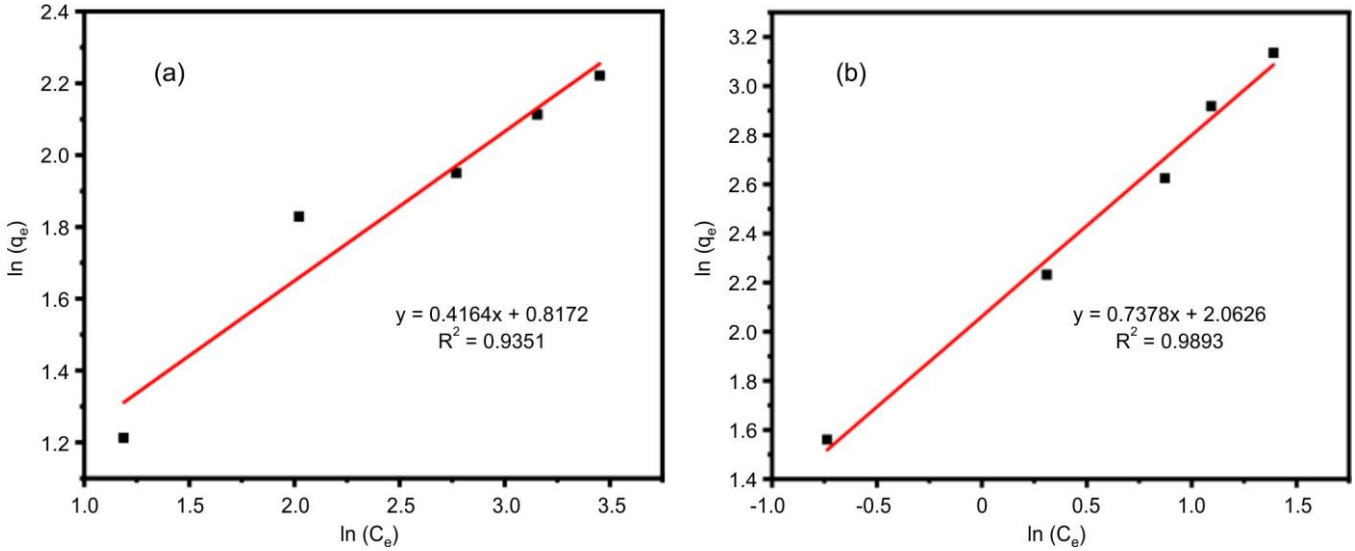

Fig. 15. Freundlich isotherm plots of CTS (a) and CTS-ZrO_2-f-MWCNTs (b)

TABLE-2
THE LANGMUIR AND FREUNDLICH MODEL PARAMETERS FOR HA ADSORPTION ONTO CTS AND CTS-ZRO_2-F-MWCNTS

Adsorbents	Isotherm models	Calculated parameters		
		q_m (mg g^{-1})	b (L/mg)	R^2
CTS	Langmuir (Type 1)	11.10	2.236	0.9871
CTS-ZrO_2-f-MWCNTs		52.09	0.178	0.7514
CTS	Langmuir (type 2)	11.14	0.135	0.9807
CTS-ZrO_2-f-MWCNTs		32.89	0.347	0.9830
CTS	Langmuir (Type 3)	10.72	0.151	0.8984
CTS-ZrO_2-f-MWCNTs		36.76	-0.302	0.659
CTS	Langmuir (Type 4)	1.836	-0.430	0.857
CTS-ZrO_2-f-MWCNTs		28.22	-0.004	0.7086
		K_f (mg g^{-1})(mg L^{-1})^n	n	R^2
CTS	Freundlich	2.264	2.402	0.9351
CTS-ZrO_2-f-MWCNTs		7.866	1.355	0.9893

TABLE-3
COMPARISON OF CTS-ZRO_2-F-MWCNTS COMPOSITE ADSORBENT WITH OTHER ADSORBENTS ON THE REMOVAL OF HA

Adsorbent	Removal efficiency (%)	Adsorption capacity (mg g^{-1})	Contact time (min)	Temp. (ºC)	pH	Ref.
CTS-Magnetite	91.50	10.98	180	25	6	[4]
CTS-ECH	95.10	8.64	110	25	4	[39]
Graphene oxide-Al	91.00	5.91	1440	25	2	[40]
Palygorskite	86.5	17	120	20	6-7	[41]
Purified Attapulgite	Not reported	32.56	60	5	6	[30]
Aminated polyacrylonitrile fibers	Not reported	16.22	30	30	3	[42]
CTS-ZrO_2-f-MWCNTs	99.04	32.89	30	25	3	This work

and adsorption sites. Furthermore, the 'n' values for CTS and CTS-ZrO_2-f-MWCNTs are 2.402 and 1.355, respectively, indicating that the adsorption sites are evenly distributed on the adsorbent surface (n > 1) [29], making the two suitable for adsorption process.

Fig. 16 shows the effect of contact time between HA and CTS adsorbents at optimal conditions. The experimental findings for every composite demonstrate that the amount of HA adsorbed increases with the duration of time the adsorbent is in contact with the HA aqueous solution, until equilibrium is attained. The highest removal efficiency of HA for CTS, CTS-ZrO_2, CTS-ZrO_2-N-doped MWCNTs and CTS-ZrO_2-f-MWCNTs are 92,56%, 96,69%, 98.16% and 99.04%, respectively. Additionally, the rate of adsorption is very high at first until equilibrium is attained, after which it plateaus or remains constant. The reason for this is that the pores and/or adsorption sites of the composites are initially vacant but as time goes on and equilibrium times are achieved, the spaces fill up and eventually become full, preventing further adsorptions [9].

Adsorption kinetics: The kinetics of the adsorption process was analyzed utilising two models: the pseudo-first order model and the pseudo-second order model [43]. The alignment of experimental results with kinetic models produces correlation coefficient values (R^2) derived from linear regression analysis, which are utilized to determine the most appropriate model fit. The pseudo first-order model, as introduced by Lagergren, is employed to characterise the adsorption phase of adsorbed HA [6]. The model is described by the following formula:

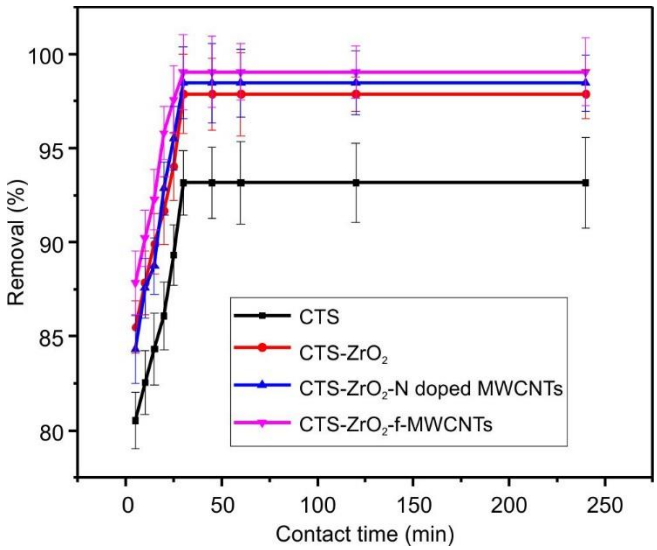

Fig. 16. Effect of contact time on the adsorption of HA from aqueous solution (experimental conditions: pH = 3; dosage, 2 g L^{-1}, HA concentration, 10 mg L^{-1}; at room temperature)

$$\ln(q_e - q_t) = \ln(q_e) - k_1 t \quad (4)$$

where q_e refers to the amount adsorbed (mg g^{-1}) per adsorbent, q_t represents the amount adsorbed (mg g^{-1}) per adsorbent at time t, k_1 is the rate constant of adsorption (min^{-1}).

The plot of ln ($q_e - q_t$) against t gives a linear relationship from which q_e can be estimated from intercept and k_1 from the slope. With a response rate determined by the total number of adsorbed species on the composite surface, the pseudo

second-order is used to distinguish adsorbed species adsorption on adsorbents [6]. The following equation describes the model:

$$\frac{t}{q_t} = \frac{1}{k_2 q_e^2} + \frac{1}{q_t} t \quad (5)$$

where k_2 is the second-order rate constant of adsorption (g mg^{-1} min^{-1}). The plot of t/q_t against t also showed a linear relationship from which k_2 was estimated from intercept and q_e from slope.

Figs. 17 and 18 show the pseudo-first order and pseudo-second order of CTS and CTS-ZrO_2-f-MWCNTs composites respectively. The pseudo first-order and second-order equations were used to calculate the adsorption parameters and the values are presented in Table-4. The pseudo first-order equation is found to be appropriate for both adsorbents, as evidenced by the correlation coefficients of 0.9365 and 0.9315 for CTS and CTS-ZrO_2-f-MWCNTs, respectively when compared to the pseudo second-order model. In addition, the calculated amount of HA adsorbed at equilibrium (q_e) for CTS and CTS-ZrO_2-

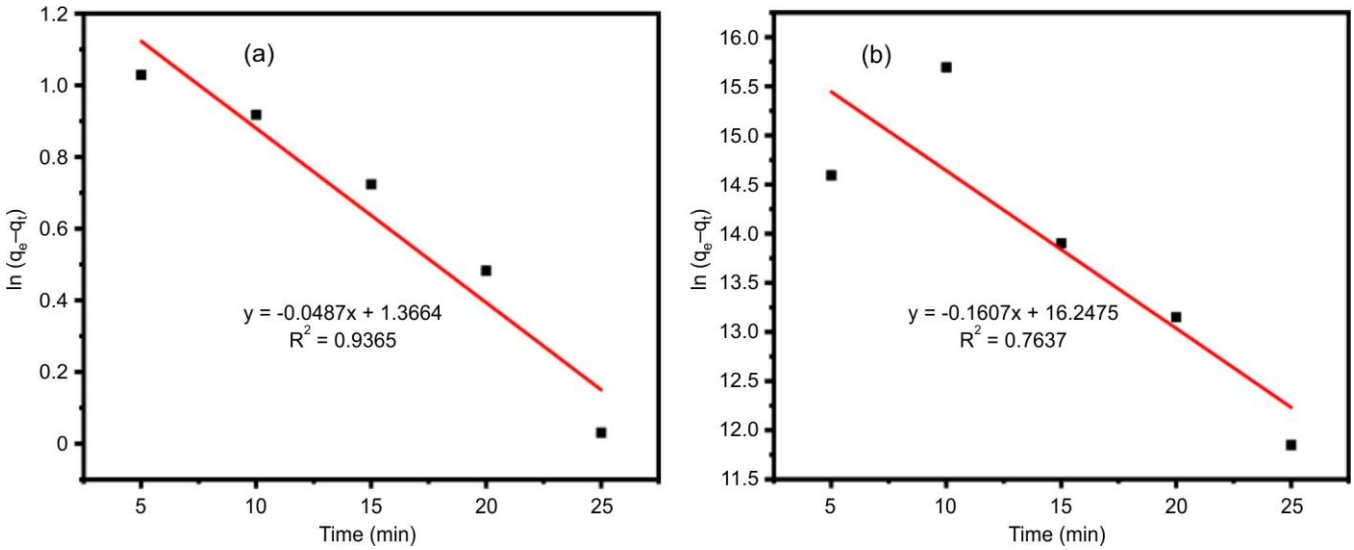

Fig. 17. Pseudo-first order (a) and second order plot (b) of CTS

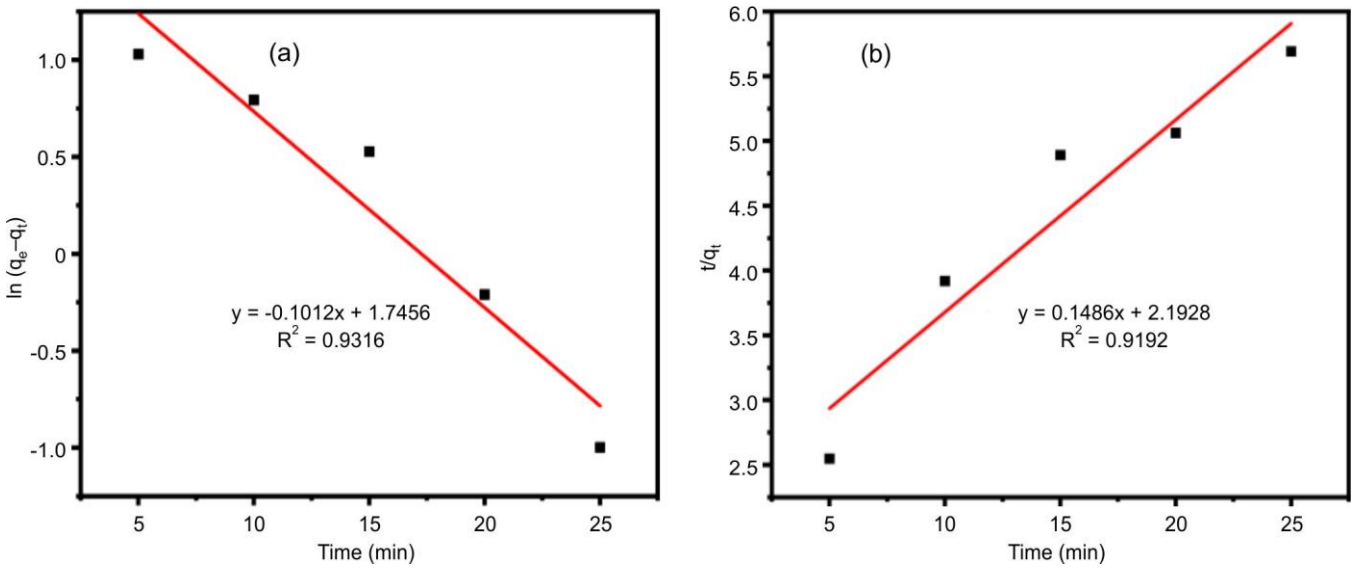

Fig. 18. Pseudo-first order (a) and second order (b) of CTS-ZrO_2-f-MWCNTs

TABLE-4
PARAMETERS OF PSEUDO FIRST-ORDER AND SECOND-ORDER MODELS FOR ADSORPTION OF HA ONTO CTS AND CTS-ZRO_2-F-MWCNTS

Adsorbents	Experimental data (q_e)	Pseudo first-order model			Pseudo second-order model		
		$-k_1$ (min^{-1})	q_e (mg g^{-1})	R^2	k_2 (g/mg.min)	q_e (mg g^{-1})	R^2
CTS	3.36	0.0486	3.92	0.9365	1.589×10^{-3}	-6.22	0.7637
CTS-ZrO_2-f-MWCNTs	4.76	0.1012	5.73	0.9315	0.01	6.73	0.9192

f-MWCNTs are 3.92 and 5.73, respectively which agree with the experimental data. Also, the computed values of q_e for the pseudo second-order model do not agree with the experimental data. These results show that the adsorption of HA from an aqueous solution onto all adsorbents obey pseudo first order which suggests that the rate of adsorption depend on the concentration of the excess adsorbate [44].

Fig. 19 shows the effect of temperature on adsorption of HA at optimal conditions. Temperature studies were conducted to determine its influence on the adsorption of HA by ranging the temperature from 25 to 40 ºC. According to Fig. 19, as temperature increases, the amount of HA adsorbed on adsorbent decreases for all adsorbents. This can be justified by solubility of HA at high temperatures of which must be overcome by breaking the water-HA strong interactions, that is, as temperature increases, solubility of HA increases and hinders adsorption [45]. Furthermore, as temperatures increases, the molecules gain high kinetic energy, resulting in a higher frequency of molecular collisions [46]. This phenomenon can lead to the displacement of adsorbed humic acid (HA) molecules from the adsorbent. The experimental results show that CTS, CTS-ZrO_2, CTS-ZrO_2-N-doped MWCNTs and CTS-ZrO_2-f-MWCNTs have high removal efficiency of 92,56%, 96,69%, 98.16% and 99.04%, respectively at standard temperature (25 ºC).

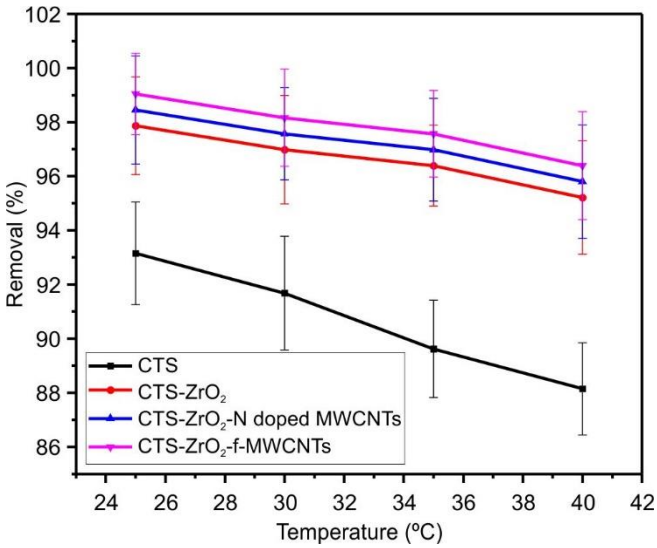

Fig. 19. Effect of temperature on the adsorption of HA on aqueous solution (experimental conditions: pH = 3; dosage, 2 g L^{-1}; initial concentration of HA, 10 mg L^{-1} and contact time, 30 min)

Thermodynamics studies: Thermodynamic analysis were conducted to examine the influence of temperature on the adsorption process [47]. There are two primary physical adsorption processes that occur in small pores, each of which is thermodynamically distinct. These two components of adsorption are (i) fluid isothermal compression and (ii) isothermal ingestion of pure adsorbents in compressed air. A thorough explanation is provided by the thermodynamic properties *viz.* ΔS^o, ΔG^o and ΔH^o) of the thermodynamic system [45]. There are other applications for the van't Hoff formula, however it does not require adherence to the physical balance chemistry principles for measuring the thermodynamic parameters of the adsorption process [48] and is as follows:

$$\ln K_C = \left(-\frac{\Delta H^o}{R}\right)\frac{1}{T} + \frac{\Delta S^o}{R} \quad (6)$$

$$\Delta G = -RT \ln K_C \quad (7)$$

$$K_C = \frac{C_s}{C_e} \quad (8)$$

where R, T and C_S (mg L^{-1}) are the universal gas constant (8.314 J mol^{-1} K^{-1}), temperature in Kelvin and the concentration of HA on the adsorbent at equilibrium, respectively. The plot of ln K_C *versus* 1/T gives a linear relationship where the values of ΔH^o and ΔS^o are calculated from the slope and the intercept, respectively.

Table-5 shows the thermodynamics parameters for the adsorption of HA onto CTS and CTS-ZrO_2-f-MWCNTs and the corresponding plot in Fig. 20. The results show a negative ΔG^o for both CTS and CTS-ZrO_2-f-MWCNTs which indicate that the adsorption of HA onto mentioned adsorbents is spontaneous under optimized experimental conditions. The exothermic characteristics of HA adsorption onto both adsorbents are evidenced by the negative values of ΔH^o. This phenomenon may be attributed to the observation that the adsorption of HA onto the adsorbents decreases as the temperature rises, meaning increasing temperature hinders adsorption which can only mean adsorption release heat [48]. The difference in ΔH^o observed between CTS and CTS-ZrO_2-f-MWCNTs suggests a significant interaction between HA and CTS-ZrO_2-f-MWCNTs. When HA is adsorbed on the composites, a higher disorder is observed at the solid-solution interface due to the positive entropy values, which shows that there are more species at the solid-liquid interface [48]. Furthermore, HA accumulates more and become more random on CTS-ZrO_2-f-MWCNTs than on CTS, which explains why the entropy value of CTS-ZrO_2-f-MWCNTs is higher than that of CTS. In other words, the adsorption of HA is enhanced in the presence of a greater number of adsorption sites on the CTS-ZrO_2-f-MWCNTs composite.

Ionic strength: Natural River waters exhibit significant quantities of Cl^-, SO_4^{2-} and NO_3^- alongside HA, which might affect its removal. These anions may engage with diverse

TABLE-5
PARAMETERS OF THERMODYNAMICS FOR THE ADSORPTION OF HA ONTO CTS AND CTS-ZRO$_2$-F-MWCNTS

Adsorbents	Temp. (K)	K_C	ΔG^o (kJ mol^{-1})	ΔH^o (kJ mol^{-1})	ΔS^o (kJ mol^{-1})
CTS	298	1.92092	-1.6174	-38.1654	0.1244
	303	1.17306	-2.9551		
CTS-ZrO_2-f-MWCNTs	298	19.9209	-7.4123	-112.0893	0.3565
	303	4.5448	-3.8139		

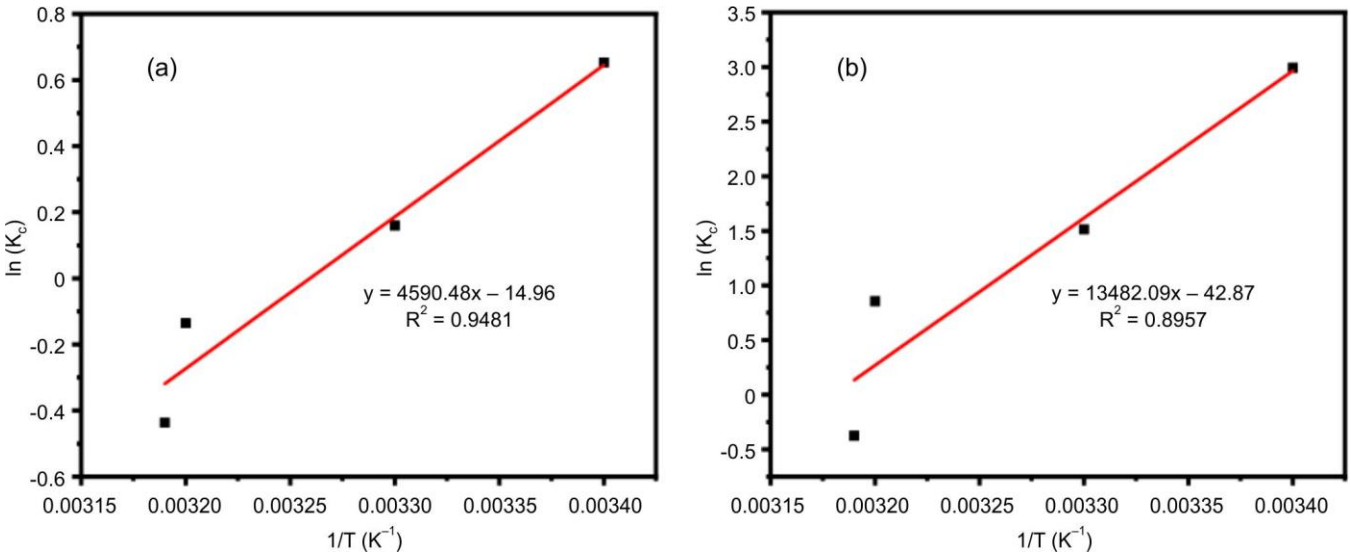

Fig. 20. Thermodynamic plot of CTS (a) and CTS-ZrO_2-f-MWCNTs (b)

ions or molecules, resulting in the synthesis of complex compounds and precipitates. Fig. 21 shows the effect of the presence of anions (Cl^-, SO_4^{2-} and NO_3^-) on the adsorption of HA onto the best adsorbing composite adsorbent, CTS-ZrO_2-f-MWCNTs. This was achieved by conducting batch adsorption of HA in the presence ions under optimal conditions, while varying the concentrations of anions from 10 to 30 ppm. The adsorbent removed 99.04% of HA in the absence of the above-mentioned anions at optimum conditions, however, as the concentration of the anions increase from 10 ppm of Cl^-, SO_4^{2-} and NO_3^- each to 30 ppm, HA removal is hindered and removal efficiency lowered to 82.55%, 62.50% and 40.43%, respectively. This can be attributed to that at pH 3, the adsorbent surface is positively charged and will form electrostatic attractions with existing anions [49]. Hence, the available anions (Cl^-, SO_4^{2-} and NO_3^-) utilise/occupy the available adsorption sites in competition with the neutral HA hence hindering its removal efficiency. It is clear that at very low anion concentrations, their effect ceases, indicating an inverse proportional relationship.

Binary system: The investigation of binary systems is essential for effective wastewater treatment, as wastewater contains many organic and inorganic contaminants that can significantly influence the adsorption of the target contaminant. Fig. 22 illustrates the influence of binary systems on the adsorption of HA, performed in the presence of casein derived from bovine milk. The results obtained show that the chosen composite adsorbent has a higher affinity towards HA than casein. This can be due to that, the adsorption parameters used are optimum for the adsorption of HA. However, the removal efficiency of HA in binary system as compared to single adsorption system, was reduced from 99.04% to 70.18% in the presence of casein. This can be attributed to that both the

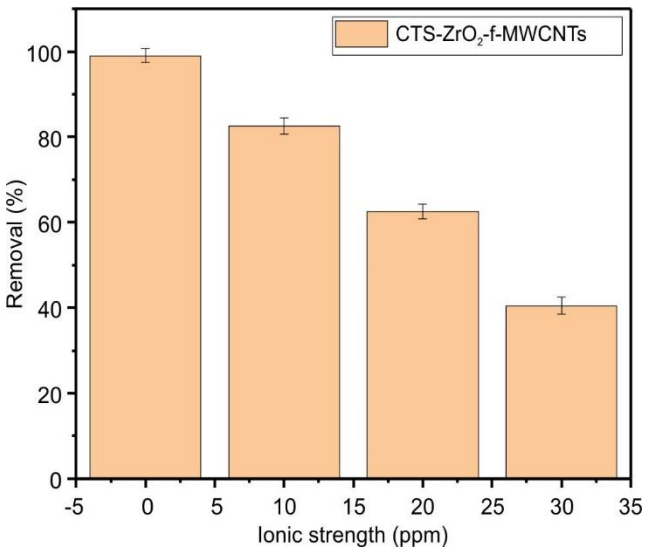

Fig. 21. Effect of ionic strength on the adsorption of HA from aqueous solution (experimental conditions: pH = 3; dosage, 2 g L^{-1}; initial concentration of HA, 10 mg L^{-1}, concentration of ions, 10, 20 and 30 mg L^{-1} of Cl^-, SO_4^{2-} and NO_3^- ions each; contact time, 30 min; and temperature, 25 ºC)

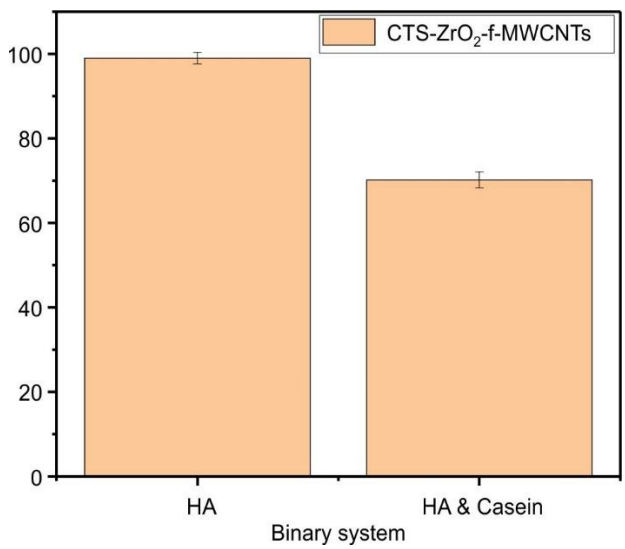

Fig. 22. Effect of binary systems (competitive) on the adsorption of HA (experimental conditions: pH = 3; dosage, 2 g L^{-1}; initial concentration of HA, 10 mg L^{-1}, concentration of Casein, 10 mg L^{-1}; contact time, 30 min; and temperature, 25 ºC)

contaminants contend for adsorption on the same adsorption sites of the composite adsorbent. Each adsorption site can bind either HA or casein molecule, but not both concurrently [50]. Notably, the results did not differ significantly between single and binary systems, suggesting that the competition between HA and casein is relatively weak despite a signify-cant influence.

Reusability studies: Fig. 23 shows the reusability of the composites for the removal of HA. In addition to having higher adsorption capacity, an ideal adsorbent should also have superior desorption properties, as this will greatly lower the adsorbents' total cost. Since the adsorption of HA onto CTS adsorbents is pH-dependent and works best at lower pH, desor-ption of HA is achieved by simply increasing pH or placing CTS composite-HA matrix in basic solution. As mentioned previously, a rise in the solution pH increases the solubility of HA, which reduces its interaction with the composite. As a result, at pH > 7, the negative charge of HA increases which leads to the higher electrostatic repulsions with composite surface; due to the deprotonation of the surface groups. The experimental results, as shown in Fig. 23, show that the composites can be effectively reused for five cycles, of which the removal efficiencies decrease slightly by 5% of CTS and CTS-ZrO_2-f-MWCNTs, respectively, of the initial removal efficiencies. This is possibly due to the partial cleavage of the link between CTS and MWCNTs or ZrO_2 and rarely HA during the regeneration process. This means that the hybrid compo-sites can be reused as highly efficient recyclable adsorption material but with less capacity than in the first cycle.

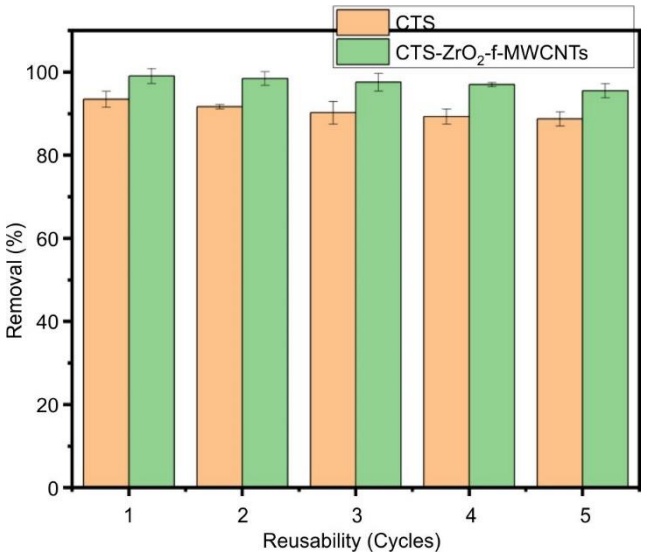

Fig. 23. Reusability of CTS and CTS-f-MWCNTs for adsorption of HA (experimental conditions: pH = 3; dosage, 2 g L^{-1}; initial concentra-tion of HA, 10 mg L^{-1}, contact time, 30 min; and temperature, 25 ºC)

Conclusion

The study focused on the adsorption of humic acid (HA) from aqueous solutions by modified CTS adsorbent. The characterisation results exhibited the potential of the CTS-ZrO_2-f-MWCNTs as a suitable adsorbent for the removal of HA from aqueous solution due to its enhance surface, showing presence of surface defects and abundant adsorption sites. The pH of the HA solution, adsorbent dosage, initial concentra-tion, contact time and temperature were optimized to highest removal efficiency of 99.04% at pH 3, dosage of 2 g L^{-1}, initial concentration of 10 ppm, reached equilibrium at 30 min contact time and at 25 ºC. Adsorption predominantly trans-pired in homogeneous monolayers and was regulated by the Langmuir model Type 2. Adsorption kinetics were found to follow pseudo-first order for both CTS and best adsorbing adsorbent CTS-ZrO_2-f-MWCNTs. Thermodynamic studies revealed the exothermic nature and thus, the spontaneity of adsorption of HA onto the adsorbents, due to a negative change in enthalpy. The synthesized adsorbents were reusable for up to 5 cycles with the reduction of 1% at each cycle. The study of the ionic strength revealed that elevated ionic strength weaken adsorption ability as the removal efficiency of HA decreased from 99.04% to 82.55%, 62.50% and 40.43%, respectively, because they occupy the adsorption sites on the composite. The competitive effect in binary systems resulted in a diminished adsorption capacity for HA, though the reduc-tion was minimal, indicating a rather modest competition for active sites on CTS-ZrO_2-f-MWCNTs. Collectively, these findings indicate that HA predominantly binds *via* physical interactions improving adsorption capacity. Adsorption tech-nique using CTS-ZrO_2-f-MWCNTs represented a promising area of research in the field of water purification, providing innovative solutions that contribute to addressing emerging water contaminants issues and improving the water quality worldwide. It provided appropriate, effective and low-cost water treatment procedure for successful water reuse. This study provides valuable insights; however, it is important to acknowledge its limitations. The work focuses on batch adsor-ption experiments conducted under controlled laboratory conditions, which may not fully reflect the complexities of real-world wastewater treatment. Therefore, further studies are needed to evaluate adsorption performance in actual water systems.

ACKNOWLEDGEMENTS

The authors express their gratitude to the National Research Foundation (NRF) for the support through NRF-Thuthuka funding (TTK2203311375).

CONFLICT OF INTEREST

The authors declare that there is no conflict of interests regarding the publication of this article.

DECLARATION OF AI-ASSISTED TECHNOLOGIES

The authors declare that no AI tools were used in the preparation or writing of this research/review article.

REFERENCES

1. A. Arumugam, K.E. Lee, P.Y. Ng, A.S. Shamsuddin, A. Zulkifli and T.L. Goh, *Emerg. Contam.*, **11**, 100470 (2025); https://doi.org/10.1016/j.emcon.2025.100470
2. R. Kumar, M. Qureshi, D.K. Vishwakarma, N. Al-Ansari, A. Kuriqi, A. Elbeltagi and A. Saraswat, *Case Stud. Chem. Environ. Eng.*, **6**, 100219 (2022); https://doi.org/10.1016/j.cscee.2022.100219

3. R.S. Das, A. Kumar, A.V. Wankhade and D.R. Peshwe, *Carbohydr. Polym.*, **278**, 118940 (2022); https://doi.org/10.1016/j.carbpol.2021.118940
4. J. Li, Y. Dai, Q. Su, B. Wang and L. Hou, *Environ. Funct. Mater*, (2025); https://doi.org/10.1016/j.efmat.2025.03.002
5. J. Wilkinson, P.S. Hooda, J. Barker, S. Barton and J. Swinden, *Environ. Pollut.*, **231**, 954 (2017); https://doi.org/10.1016/j.envpol.2017.08.032
6. B.S. Rathi and P.S. Kumar, *Environ. Pollut.*, **280**, 116995 (2021); https://doi.org/10.1016/j.envpol.2021.116995
7. R.S. Ribeiro, R.O. Rodrigues, A.M.T. Silva, P.B. Tavares, A.M.C. Carvalho, J.L. Figueiredo, J.L. Faria and H.T. Gomes, *Appl. Catal. B*, **219**, 645 (2017); https://doi.org/10.1016/j.apcatb.2017.08.013
8. A. Rao, A. Kumar, R. Dhodapkar and S. Pal, *Environ. Sci. Pollut. Res. Int.*, **28**, 21347 (2021); https://doi.org/10.1007/s11356-020-12014-1
9. S. Li, M. He, Z. Li, D. Li and Z. Pan, *J. Mol. Liq.*, **230**, 520 (2017); https://doi.org/10.1016/j.molliq.2017.01.027
10. M. Sabri, H. Kazim, M. Tawalbeh, A. Al-Othman and F. Almomani, *Chemosphere*, **365**, 143373 (2024); https://doi.org/10.1016/j.chemosphere.2024.143373
11. S. Wang and Z.H. Zhu, *J. Colloid Interface Sci.*, **315**, 41 (2007); https://doi.org/10.1016/j.jcis.2007.06.034
12. R. Khakpour and H. Tahermansouri, *Int. J. Biol. Macromol.*, **109**, 598 (2018); https://doi.org/10.1016/j.ijbiomac.2017.12.105
13. A. Munwana and L.E. Macevele, *Dig. J. Nanomater. Biostruct.*, **20**, 227 (2025); https://doi.org/10.15251/DJNB.2025.201.227
14. M. Nazaripour, M.A.M. Reshadi, S.A. Mirbagheri, M. Nazaripour and A. Bazargan, *J. Environ. Manage.*, **287**, 112322 (2021); https://doi.org/10.1016/j.jenvman.2021.112322
15. M. Keshvardoostchokami, M. Majidi, A. Zamani and B. Liu, *Carbohydr. Polym.*, **273**, 118625 (2021); https://doi.org/10.1016/j.carbpol.2021.118625
16. M.A. Kaczorowska and D. Bożejewicz, *Sustainability*, **16**, 2615 (2024); https://doi.org/10.3390/su16072615
17. K.A. Omran, M.R. El-Aassar, O.M. Ibrahim, S.A. Sharaewy, R.E. Khalifa and F.M. Mohamed, *Desalination Water Treat.*, **317**, 100294 (2024); https://doi.org/10.1016/j.dwt.2024.100294
18. M.S. Rostami and M.M. Khodaei, *Int. J. Biol. Macromol.*, **270**, 132386 (2024); https://doi.org/10.1016/j.ijbiomac.2024.132386
19. M. Vakili, M. Rafatullah, B. Salamatinia, A.Z. Abdullah, K.B. Tan, M.H. Ibrahim, Z. Gholami and P. Amouzgar, *Carbohydr. Polym.*, **113**, 115 (2014); https://doi.org/10.1016/j.carbpol.2014.07.007
20. K. Mohan, D. Karthick Rajan, J. Rajarajeswaran, D. Divya and A. Ramu Ganesan, *Curr. Opin. Environ. Sci. Health*, **33**, 100473 (2023); https://doi.org/10.1016/j.coesh.2023.100473
21. J. Jin, H. Zhang, A.A. Aryee, Y. Wang, R. safdar, W. Shi, L. Qu and R. Han, *Int. J. Biol. Macromol.*, **320**, 144779 (2025); https://doi.org/10.1016/j.ijbiomac.2025.144779
22. S.S. Elanchezhiyan, N. Sivasurian and S. Meenakshi, *Carbohydr. Polym.*, **145**, 103 (2016); https://doi.org/10.1016/j.carbpol.2016.02.038
23. S. Sonal and B.K. Mishra, *Chem. Eng. J.*, **424**, 130509 (2021); https://doi.org/10.1016/j.cej.2021.130509
24. R.S. Das, S.K. Warkhade, A. Kumar and A.V. Wankhade, *Res. Chem. Intermed.*, **45**, 1689 (2019); https://doi.org/10.1007/s11164-018-3699-z
25. A. Khazaie, H. Kia, E. Moniri, A.H. Hassani and M. Miralinaghi, *J. Taiwan Inst. Chem. Eng.*, **144**, 104743 (2023); https://doi.org/10.1016/j.jtice.2023.104743
26. L.P.L. Gonçalves, M. Meledina, A. Meledin, D.Y. Petrovykh, J.P.S. Sousa, O.S.G.P. Soares, Y.V. Kolen'ko and M.F.R. Pereira, *Carbon*, **195**, 35 (2022); https://doi.org/10.1016/j.carbon.2022.03.059
27. K. Azlan, W.N. Wan Saime and L. Lai Ken, *J. Environ. Sci. (China)*, **21**, 296 (2009); https://doi.org/10.1016/S1001-0742(08)62267-6
28. M. Khodakarami and R. Honaker, *J. Hazard. Mater. Adv.*, **912**, 169519 (2024); https://doi.org/10.1016/j.scitotenv.2023.169519
29. L.L. Borba, R.M.F. Cuba, F.J. Cuba Terán, M.N. Castro and T.A. Mendes, *Brazilian Arch. Biol. Technol.*, **62**, (2019); https://doi.org/10.1590/1678-4324-2019180450
30. N. Sun, Y. Zhang, L. Ma, S. Yu and J. Li, *J. Taiwan Inst. Chem. Eng.*, **78**, 96 (2017); https://doi.org/10.1016/j.jtice.2017.03.017
31. N.F. Shoparwe, L.C. Kee, T.A. Otitoju, H. Shukor, N. Zainuddin and M.M.Z. Makhtar, *Membranes (Basel)*, **11**, 721 (2021); https://doi.org/10.3390/membranes11090721
32. L.E. Macevele, K.L.M. Moganedi and T. Magadzu, *J. Compos. Sci.*, **8**, 119 (2024); https://doi.org/10.3390/jcs8040119
33. N.B. Mkhondo and T. Magadzu, *Dig. J. Nanomater. Biostruct.*, **9**, 1331 (2014).
34. M. Kosmulski, *Adv. Colloid Interface Sci.*, **319**, 102973 (2023); https://doi.org/10.1016/j.cis.2023.102973
35. N.V. Perez-Aguilar, E. Muñoz-Sandoval, P.E. Diaz-Flores and J.R. Rangel-Mendez, *J. Nanopart. Res.*, **12**, 467 (2010); https://doi.org/10.1007/s11051-009-9670-6
36. T. Zhou, S. Huang, D. Niu, L. Su, G. Zhen and Y. Zhao, *ACS Sustain. Chem.& Eng.*, **6**, 5981 (2018); https://doi.org/10.1021/acssuschemeng.7b04507
37. A.A.M. Daifullah, B.S. Girgis and H.M.H. Gad, *Colloids Surf. A Physicochem. Eng. Asp.*, **235**, 1 (2004); https://doi.org/10.1016/j.colsurfa.2003.12.020
38. R. Kecili, C.M. Hussain, *Elsevier Inc.*, (2018); https://doi.org/10.1016/B978-0-12-812792-6.00004-2
39. N. Hilmioglu and E. Yumat, *Water Air Soil Pollut.*, **235**, 293 (2024); https://doi.org/10.1007/s11270-024-07044-1
40. A.K. Tolkou, I.A. Katsoyiannis and G.Z. Kyzas, *J. Compos. Sci.*, **9**, 327 (2025); https://doi.org/10.3390/jcs9070327
41. M. Wang, L. Liao, X. Zhang and Z. Li, *Appl. Clay Sci.*, **67–68**, 164 (2012); https://doi.org/10.1016/j.clay.2011.09.012
42. S. Deng and R. Bai, *J. Colloid Interface Sci.*, **280**, 36 (2004); https://doi.org/10.1016/j.jcis.2004.07.007
43. G. Moussavi, S. Talebi, M. Farrokhi and R.M. Sabouti, *Chem. Eng. J.*, **171**, 1159 (2011); https://doi.org/10.1016/j.cej.2011.05.016
44. C. Zhang, J. Sui, J. Li, Y. Tang and W. Cai, *Chem. Eng. J.*, **210**, 45 (2012); https://doi.org/10.1016/j.cej.2012.08.062
45. L.E. Macevele, K. Lydia, M. Moganedi, T. Magadzu, *J. membr. sci. res.*, **7**, 152 (2021); https://doi.org/10.22079/JMSR.2020.121858.1351
46. M.A. Islam, D.W. Morton, B.B. Johnson and M.J. Angove, *Separ. Purif. Tech.*, **247**, 116949 (2020); https://doi.org/10.1016/j.seppur.2020.116949
47. G. Limousin, J.P. Gaudet, L. Charlet, S. Szenknect, V. Barthès and M. Krimissa, *Appl. Geochem.*, **22**, 249 (2007); https://doi.org/10.1016/j.apgeochem.2006.09.010
48. X. Hu and Z. Cheng, *Chin. J. Chem. Eng.*, **23**, 1551 (2015); https://doi.org/10.1016/j.cjche.2015.06.010
49. X. Wei, Y. Shi, Y. Fei, J. Chen, B. Lv, Y. Chen, H. Zheng, J. Shen and L. Zhu, *Chem. Eng. J.*, **292**, 382 (2016); https://doi.org/10.1016/j.cej.2016.02.037
50. L. Sellaoui, F.E. Soetaredjo, N. Sghaier, A. Erto, T. Saidani, N. Alwadai, M. Badawi, G.L. Dotto and S. Ismadji, *Appl. Clay Sci.*, **276**, 107922 (2025); https://doi.org/10.1016/j.clay.2025.107922